Università
Ca'Foscari
Venezia

Corso di Dottorato di ricerca

in Science and Management of Climate Change

ciclo 32

Tesi di Ricerca

in cotutela con il Centro Euro-Mediterraneo sui Cambiamenti Climatici (CMCC)

The Kuroshio Extension low frequency variability:

the relative roles of internal and external drivers

SSD: GEO12

Coordinatore del Dottorato
ch. prof. Carlo Carraro

Supervisore
ch. prof. Simona Masina

Supervisore cotutela
ch. prof. Alessio Bellucci

Supervisore cotutela
ch. prof. Stefano Pierini

Dottorando
Giusy Fedele

Matricola
956305

“Swing away

Merrill”

Contents

Chapter 1

1. Introduction

1.1 Motivation

This thesis is devoted to the study of the Kuroshio Extension (KE) system. The KE is the eastward inertial meandering jet formed after the separation of the Kuroshio and Oyashio western boundary currents (WBCs) East of Japan at around 35°N, 142°E; it constitutes, therefore, a front separating the warm subtropical and cold subpolar waters of the Northwest Pacific. The KE region has the largest sea surface height (SSH) variability on interannual time scales in the extratropical North Pacific Ocean (Qiu 2002) and the highest eddy kinetic energy levels in the Northern Pacific in which large-scale interannual changes lead to high sea surface temperature (SST) anomalies that are capable of enhancing the variability of the midlatitude coupled ocean–atmosphere system (Xie et al. 2000). This feedback on SST occurs in winter when a deep mixed layer develops by vertical entrainment (Schneider et al. 2002) or horizontal advection by the varying KE (Qiu 2000; Seager et al. 2001; Tomita et al. 2002; Scott and Qiu 2003). Therefore, the ocean has an active role in the KE region in enhancing perturbations in the atmosphere (Bishop et al., 2017); for instance, an evidence is provided by Zhang and Luo (2017), who observed that changes in the KE can lead to changes in the location and strength of the North Pacific storm track.

The KE jet undergoes relevant variations on interannual -to- decadal time scale (Qiu, 2002; Qiu and Chen; 2010). This low frequency variability (LFV) connects a zonally elongated, fairly stable and energetic meandering jet and a much weaker, highly variable and convoluted jet with a reduced zonal penetration (hereafter called elongated and convoluted modes, respectively).

The nature of this variability is still under debate and poorly understood, motivating many scientists to explore in detail the mechanisms that play a role in the phenomenon.

It is important from a climatic point of view to understand the mechanisms behind the KE LFV to assess the ability of the state-of-the-art models to capture the variability of the jet and to improve our understanding of the predictability of this dynamical system.

1.2 Goals and methods

The KE oscillates between two main states led by mechanisms whose nature is still poorly understood and under debate. The debate is focused on the role of intrinsic variability and external forcing in driving the quasi-decadal variability of the jet. To this respect, many authors have suggested that nonlinear intrinsic oceanic mechanisms (i.e., those not directly induced by the atmospheric variability) can play a fundamental role in the phenomenon (e.g., for a review of idealized modelling studies in this context see Dijkstra and Ghil, 2005; Pierini 2006; 2014); but in contrast, the KE LFV is also found to be in synchrony with the Pacific Decadal Oscillation (PDO) which takes place several thousand of kilometers east of the KE region: the teleconnection mechanism is provided by westward travelling baroclinic Rossby wave trains excited in the PDO center of action (Fig.1).

Therefore, there is still an open question on the nature of the KE LFV:

What is the role of the internal oceanic mechanisms and external atmospheric forcing in driving the KE variability?

Chapter 2 is devoted to investigate these processes, taking advantage of the OCCIPUT dataset provided by the Institut des Géosciences de l'Environnement (IGE) made of an ensemble of 50 global ocean–sea-ice hindcasts (hereafter OCCITENS), performed over the period 1960–2015 at eddy-permitting resolution (1/4°) and a one-member 330-yr climatological simulation (hereafter OCCICLIM). In this context, OCCITENS is built in order to simulate simultaneously both contributions (intrinsic and forced) and to allow their separation via ensemble statistics; while by construction OCCICLIM provides a measure of the pure intrinsic variability of the jet. In this modeling framework, the ensemble mean can be taken as an estimate of the forced, deterministic variability, induced by the atmospheric boundary conditions shared by all the members. The spread about the ensemble mean, as measured by the ensemble standard deviation and the ensemble probability density function, gives an estimate of the intrinsic, chaotic variability generated by the turbulent ocean at eddy-permitting resolution.

The OCCIPUT ensemble has never been used before to study the KE LFV and provides the ideal framework for understanding the role of the intrinsic variability and forced variability in modulating the KE jet. Taking advantage of this dataset, I investigated the KE LFV from a dynamical systems viewpoint, making a step forward into assessing the role of the

intrinsic and the forced components in the total variability of the jet.

This part aims not only to directly answer the question above, but also to make a step forward in the predictability of the KE LFV. In this thesis the predictability of this dynamical system is only mentioned, suggesting some methods that should be applied in a future work.

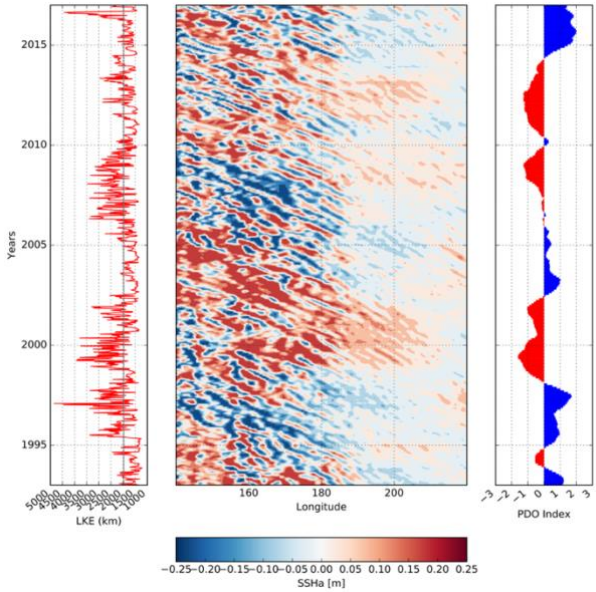

Fig.1. AVISO data. (Left) The LKE from 1993 to 2017 yrs (red line) and its mean value (in grey). (Center) The Hovmöller Diagram for the SSH anomalies in the upstream and downstream KE region [averaged between 32-34°N as Qiu and Chen, 2005]. (Right) The PDO Index computed as Newman et al., 2016.

The ocean-driven and atmospherically paced variabilities are here investigated without taking into account the air-sea feedbacks since the ocean by construction is a passive system in the OCCIPUT dataset. Therefore, to avoid neglecting the processes that may be important for this study, a good strategy would be to investigate a global coupled ocean-atmosphere general circulation model (GCM). To assess the interplay between the ocean and the atmosphere in the KE region aims to identify the oceanic-driven and atmospheric-driven regimes at different spatial and temporal scales. In fact, as already mentioned, the KE LFV strongly affects

the mid-latitude coupled ocean-atmosphere system and it is also found to be lag-correlated with the PDO. In this context, several studies show the importance to simulate mesoscale eddies in order to correctly assess the impact on the atmosphere. What is still lacking in the literature is the impact of the horizontal resolution of the atmospheric component on the main features of the KE jet and on its variability on quasi-decadal timescales. Changes in the KE jet due to changes in the horizontal resolution of the atmosphere (with the ocean model resolution unchanged) would impact on the main frontal-scale and broad-scale features and variabilities of the jet, affecting also the air-sea feedbacks.

Therefore, the second part of this thesis (chapter 3) is devoted to answer the following question:

What is the impact of the ocean-atmosphere coupling when different horizontal resolutions are adopted in the atmospheric model?

The role of horizontal resolution of the atmospheric model in a coupled model configuration has been inspected in the PRIMAVERA project framework. The model data analyzed in this part are from HIGHRESMIP-CMIP6 and are provided by the Euro-Mediterranean Center on Climate Change (CMCC).

In this context, the effects of different resolutions on the KE LFV are shown, both in terms of frontal-scale variability and broad-scale variability, making a step forward into assessing the role of the horizontal atmospheric resolution on the degree of realism of the KE jet.

Understanding the ability of the state-of-the-art models to capture the KE LFV in dependence of the resolution of the atmospheric component in

a global fully coupled model helps to identify also what are the main processes leading the LFV in the KE region and to better define the needs of the future modelling configurations.

1.3 Background

The KE phenomenology is linked to several factors: the inertial effects, the bottom topography, the coastline geometry, the stratification etc. (i.e. Kawai, H., 1972; Hurlburt et al., 1996; Pierini, 2006; 2008). The Kuroshio and Oyashio currents are very different WBCs, both for their physical and dynamical properties. In fact, the Oyashio current moving from polar latitudes transports cold and dense water equatorward, while the Kuroshio moving in the opposite direction transports warm water toward mid-latitudes. Due to the inversion of the circulation in the convergence zone and the different physical properties, the KE constitutes an oceanic front well captured by the potential density, potential temperature and salinity diagrams (Fig.2) along a KE's transect.

The upstream KE is sometimes characterized by two quasi-stationary meanders with their ridges located at 144°E and 150°E, respectively. These meanders constitute a mean circulation feature of the KE, in fact they can be observed in the sea surface dynamic height maps derived by historical hydrographic data (e.g., Wyrtki, 1975; Teague et al., 1990; Qu et al., 2001) and satellite altimeter data (Fig. 3). Near 159°E, the KE encounters the Shatsky Rise bifurcating in two branches, the main one continues eastward, and the secondary branch joins the eastward flowing Subarctic Current. East of the dateline, it is no longer clear the distinction between the KE and the

Subarctic Current, forming the broad, eastward-moving North Pacific Current (e.g., Joyce, 1987; Joyce and Schmitz, 1988; Roden, 1998; Qiu, 2002).

The KE is also known for its variability on interannual -to- decadal timescales, shifting between two contrasting modes that may be verified by simply inspecting the observed SSH maps (Fig.3). Many of the characteristics that distinguish the two modes, such as the zonal penetration of the KE jet and the intensity of the recirculation gyre, can be visually confirmed in the SSH maps computed by Qiu and Chen (2005). Analyzing the timeseries from 10/1992 to 12/2004 they show the bimodality of the jet in the altimeter data provided by many satellite missions: Topex/Poseidon (Ocean Topography Experiment), Jason- 1 and ERS-1/2 (European Remote Sensing Satellite).

The upstream and downstream LFV differ due to the different mechanisms which take place in these regions. Most of the interannual -to-decadal variability is captured from the upstream jet, therefore most of the analyses shown in this thesis are focused in this region.

During the period 1993/94 the SSHa is quite similar to the climatological field with two well defined quasi-stationary meanders east of Japan, the jet is therefore zonally elongated and fairly stable (elongated state). During the years 1995-1996 the two meanders weaken and in 1997 they dissipate in an inverse energy cascade process. The jet is zonally contracted, much more convoluted and shifted southward (convoluted state). Several indices are used to capture the KE LFV such as the KE path length (LKE), the mean latitudinal position ($<\varphi>$) of the jet and the eddy kinetic energy level (EKE). Qiu and Chen (2005) found a connection between these indices computed in the upstream region; shifting from the elongated to the convoluted states the jet moves southward, and the two quasi-stationary meanders dissipate

forming many more eddies. From their interaction the EKE and the LKE increase (Fig.4). In contrast, in the downstream region these indices are not coherent to each other as before because the jet is far away from the coast and interacts with the Shatsky Rise (Fig.5). For instance, comparing Fig.4 and Fig.5 during the years from 2001 to 2004, the EKE level is not followed by an increase of the LKE in the downstream jet as in the upstream jet. Instead the mean latitudinal position variability is pretty well captured by both, suggesting that this index captures a broad-scale feature of the KE jet, while the EKE and the LKE highlight the frontal scale variability of the system, strongly affected by the eddy-eddy interactions and therefore by the nonlinear internal oceanic mechanisms.

These indices are widely used in the next chapters to evaluate the role of the intrinsic and forced variabilities in the total variability of the jet on interannual -to- decadal timescales and also for assessing the impact of the horizontal resolution of the atmospheric model on the degree of realism of the KE dynamical system.

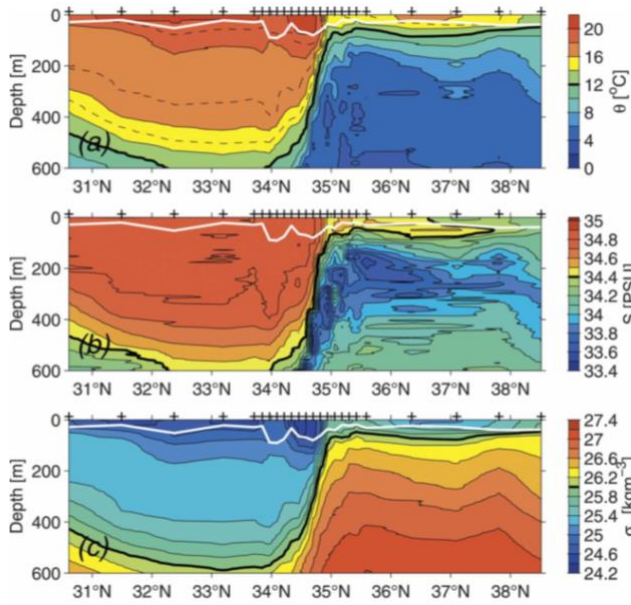

Fig.2. (a) Potential temperature, (b) salinity and (c) potential density along a transect across the KE system. Crosses at top of each panel indicate the CTD casts along the transect. White contours in (a)–(c) denote the mixed later depth, defined as the depth at which σ_θ increases by 0.125 kg m-3 from its surface value. Thick contours indicate the isopleths of (a) T=12°C, (b) S=34.4 psu, (c) σ_θ=26.0, respectively (adapted by Qiu et al.,2006).

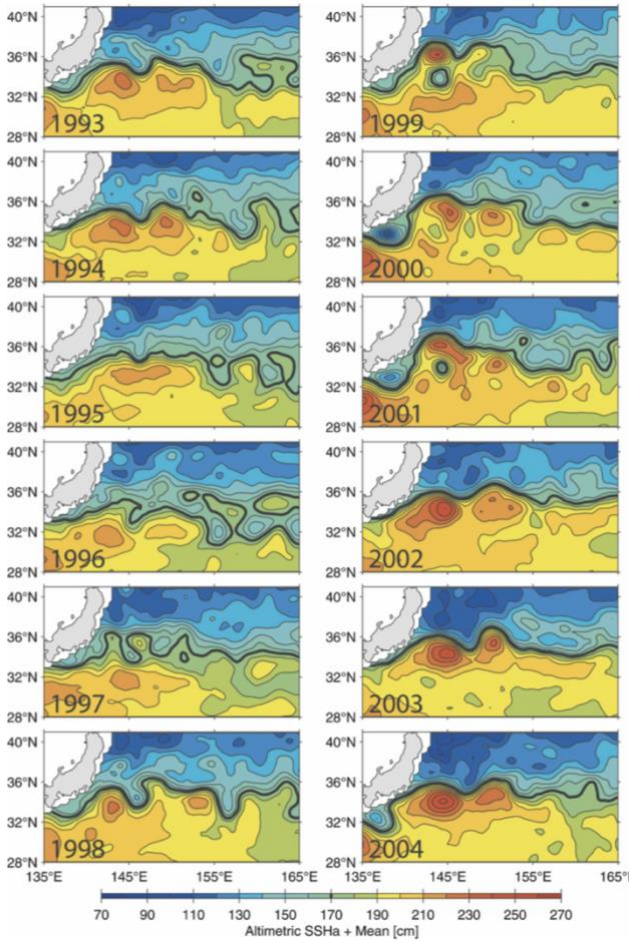

Fig.3. Maps of yearly averaged sea surface height field. Contour intervals are 10 cm with the thick lines denoting the 170-cm contours (adapted by Qiu and Chen, 2005).

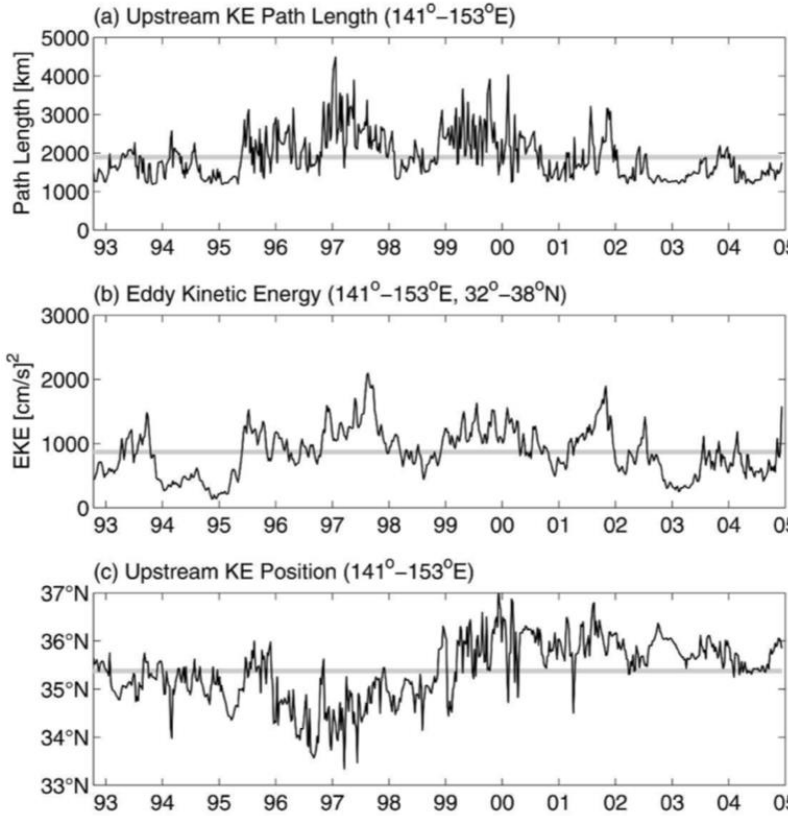

Fig. 4. (a) Upstream KE path length integrated from 141° to 153°E. (b) Eddy kinetic energy in the upstream KE region of 32°–38°N and 141°–153°E. (c) Latitudinal position of the KE averaged from 141° to 153°E. Gray lines denote the mean values of the quantity over the period of analysis (adapted by Qiu and Chen, 2005).

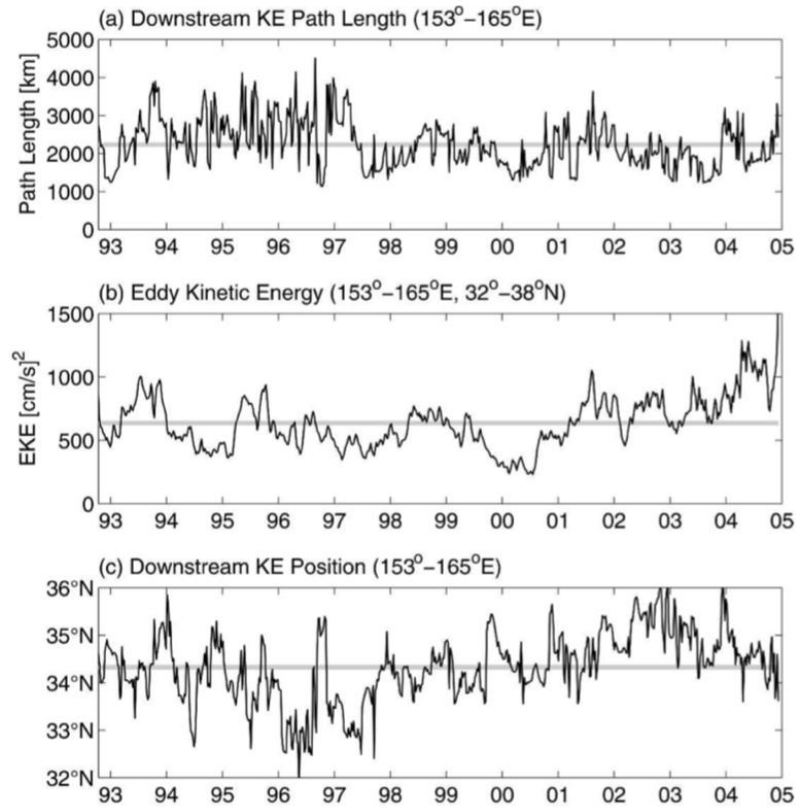

FIG. 5. Same as Fig. 3 but for the downstream KE jet (153°–165°E; adapted by Qiu and Chen, 2005).

Chapter 2

2. Interannual-to-decadal variability of the Kuroshio extension: Analyzing an ensemble of global hindcasts from a Dynamical Systems viewpoint.

2.1 Introduction

The Kuroshio Extension (KE) is the eastward flowing meandering jet formed by the confluence of the Kuroshio and Oyashio western boundary currents (WBCs) east of Japan. The KE region is known for the highest Eddy Kinetic Energy (EKE) level in the North Pacific Ocean (Wyrtki et al. 1976), whose changes lead to high temperature anomalies that are able of enhance the variability of the midlatitude coupled ocean–atmosphere system (e.g, Latif and Barnett 1994, 1996; Zhang and Luo, 2017).

It is widely mentioned in the literature that the KE variability is bimodal on interannual to decadal time scales (e.g. Chao, 1984; Qiu, 2000; 2002), shifting between two main states: the elongated state when the jet is fairly stable, zonally elongated yielding two anticyclonic meanders east of Japan and the contracted state when the jet is zonally contracted, much more convoluted and when the two anticyclonic meanders dissipate in an inverse cascade energy process (Qiu and Chen, 2005; 2010). It has also been observed that the KE's low frequency variability (LFV) can affect the location and strength of the North Pacific storm track (O'Reilly and Czaja, 2015; Zhang and Luo, 2017) and some studies also report impacts of the KE LFV on the Asian and North American Climate (e.g., Latif and Barnett 1994, 1996; Qiu 2000). It is therefore important to understand the nature of this

bimodality and to investigate the predictability properties of the phenomenon.

The nature of the KE LFV is still under debate with complementary views regarding the respective roles of the ocean's intrinsic variability and the atmospheric variability in driving the quasi-decadal variability of the jet. The first school of thought supports the idea that the KE LFV is an intrinsic mechanism influenced by nonlinear interactions between recirculations, potential vorticity advection and eddies (e.g. Jiang et al., 1995 and Dijkstra and Ghil, 2005; Pierini, 2006). Using simple double-gyre idealized models, forced by constant winds, previous studies (e.g. Schmeits & Dijkstra, 2001; Dijkstra and Ghil, 2005; Pierini, 2006) found the two KE LFV regimes in agreement with altimeter maps (as Qiu, 2003; Qiu and Chen, 2005; 2010). They interpret the mechanism which leads the shift from the elongated state to the convoluted one as linked to the eastward propagation of potential vorticity anomalies from the western boundary current region (Cessi et al., 1987). According to these theories, Dewar (2003) and Hogg et al. (2005) identified a mode of intrinsic variability, which is characterized by a slow adjustment in the potential vorticity and a meridional shift in the jet position on decadal timescales.

The intrinsic nature of the KE LFV is strongly highlighted from Pierini (2006), who used a reduced-gravity primitive equation ocean model implemented in a box spanning the whole North Pacific, which includes a schematic coastline at the western side, and an analytical wind forcing; it was thus shown that this idealized model captures the observed KE LFV (as Qiu and Chen, 2005) supporting the intrinsic origin of the phenomenon.

In contrast, the second school of thought supports the role of broad-scale atmospheric variability such as the Pacific Decadal Oscillation-PDO in inducing the KE LFV (e.g., Miller et al. 1998; Deser et al. 1999; Qiu 2003; Qiu and Chen 2005). In this context, through an eddy-resolving ocean general circulation model (OGCM), Taguchi et al. (2007) have confirmed that the KE LFV can be linked to the propagation of Rossby waves from the East-Central Northern Pacific driven by large-scale atmospheric variability. However, it has also been shown that frontal-scale variability contributes to changes in the KE jet speed, which can be generated by internal ocean dynamics, highlighting that while the linear Rossby wave theory explains the temporal variability, nonlinear ocean dynamics organize the spatial structure (Taguchi et al., 2007; Nonaka et al., 2012). These two views could be reconciled according to Pierini (2014), who interpreted the KE LFV as a case of intrinsic variability paced by an external forcing.

Nonaka et al. (2012) have investigated the potential predictability of interannual variability in the KE jet speed related to the westward propagation of wind-driven oceanic Rossby waves through prediction experiments with an eddy-resolving OGCM under the perfect-model assumption. In this framework, they observed a modest predictability on interannual timescale of the KE jet speed (only 46 % of its total variance) explained by the Rossby waves propagation. They suggested two possible reasons for the limited predictability: the influence of wind variations in the western portion of the North Pacific basin, which can reduce predictability with longer lead time and the presence of internal variability of KE jet that is uncorrelated with atmospheric forcing, and can yield randomness in the KE jet variability.

In this work we investigate the role of the intrinsic and forced components in the KE LFV, with a new approach: we analyze a large ensemble of eddy-permitting ocean/sea-ice global hindcasts and a one-member very long climatological simulation from the Dynamical Systems theory point of view. This dataset suits our purposes, because by construction, the large ensemble simulates simultaneously both contributions (intrinsic and forced) and allows their separation via ensemble statistics, while the one-member very long climatological simulation provides the quasi-autonomous (or "pure") intrinsic variability of the jet. In this modeling framework, the ensemble mean can be taken as a first estimate of the forced, deterministic variability induced by the atmospheric boundary conditions shared by all the members. The spread about the ensemble mean, as measured by time-varying ensemble standard deviations and ensemble probability density functions, gives a first estimate of the intrinsic and chaotic variability generated by the turbulent ocean at this eddy-permitting resolution.

In this work, through the dynamical systems theory, we assess the role of the internal variability and external forcings in driving the quasi-decadal variability of the jet.

Following this strategy, we not only disentangle the intrinsic component to the forced one, but we also provide the attractor of the KE jet in an autonomous and nonautonomous dynamical system (Hilborn R.C., 2000). This approach gives some advantages: it provides in the autonomous system the phase-space of the pure intrinsic variability, highlighting the main clusters populated by the jet and the comparison between the autonomous and nonautonomous systems provides not only the role of the atmosphere in

pacing the KE LFV but also a measure of the predictability of the system in the phase-space linked with the external forcings. Separating the forced and intrinsic variabilities through ensemble mean and standard deviations is a preliminary approach, which is often done in these kinds of studies. The objective of this study is to go beyond this simple approach: we will no longer assume the separability of both components, but we analyze the combined influences of the ocean's intrinsic variability and external forcing using the full probability density functions (PDFs) of the non-autonomous dynamical system.

2.2 Datasets, post-processing and model assessment

2.2.1 Datasets

We make use of two eddy-permitting (1/4°) global ocean/sea-ice simulations produced during the OCCIPUT (Oceanic Chaos – Impacts, Structure, Predictability) project (Penduff et al., 2014; Bessières et al., 2017): a large 50-member ensemble hindcast (hereafter OCCITENS) performed over the period 1960–2015, and a one-member 330-yr long climatological simulation (hereafter OCCICLIM). Both simulations were performed using the same NEMO3.5 model setup and configuration, with the same 1/4° horizontal resolution (~27km at the equator, decreasing poleward) and the same 75-level vertical discretization. OCCITENS and OCCICLIM differ by their atmospheric forcing. All members of the OCCITENS ensemble are forced by the same DRAKKAR forcing set DFS5.2 (Dussin et al. 2016), which is based on the ERA-40 and ERA-Interim reanalyses and includes the full range of atmospheric timescales over this period. OCCICLIM is forced

during the 330 years by a repeated annual cycle devoid of any interannual or synoptic variability and provides insight into the pure intrinsic variability that spontaneously emerges from the ocean. The differences between both simulations are summarized in Table 1. More details are given in Leroux et al. (2018) where these simulations are labeled as ENSx50-occi025 and CLIM-occi025.

Starting from a one-member 21-yr spinup simulation, the 50 members of the OCCITENS ensemble hindcast are generated in 1960 by activating a small stochastic perturbation in the equation of state within each member (Brankart et al. 2015; Bessières et al. 2017). This stochastic perturbation is only applied for the first year (1960) to seed the ensemble dispersion, and remains switched off for the rest of the ensemble hindcast (from 1961 to 2015). Once the stochastic perturbation is stopped at the end of 1960, the 50 members are thus integrated from slightly perturbed initial conditions and forced by the same atmospheric conditions. Our diagnostics are performed from 5-daily simulated sea-surface height (SSH) fields over the 1980–2015 period, that is, after a total effective spinup time of 41 years in each member.

Characteristics of the model used in this study: OCCIPUT		
	OCCITENS	**OCCICLIM**
Domain	Global	Global
Type	Ensemble hindcast	Climatology
No. of members N	50	1
Time period	1960-2015	330 yr
NEMO version	3.5	3.5
Resolution	1/4 ° and 75 vertical levels	1/4 ° and 75 vertical levels
Atmospheric forcing	DFS5.2 (all time scales)	Climatology from DFS4
		Reference: Bessières et al. (2017)

TABLE 1. Model setups and simulations.

The OCCITENS sea-level variability is assessed against the AVISO dataset (Archiving, Validation, and Interpretation of Satellite Oceanographic data; see AVISO webpage, http://www.aviso.altimetry.fr, and the User Handbook) which provides daily sea level anomaly (SLA) data on a 0.25-degree grid on the 1993-2017 period. Adding the Mean Absolute Dynamic Topography (MADT) provided by AVISO to these SLA fields provided observed SSH fields. The next section presents how the observed and simulated SSH fields were post-processed and used to derive additional variables and indices.

2.2.2 Post-processing

i) Indices

The altimeter maps (Fig.2) show a clear bimodal behavior of the KE, shifting between two states: one with a fairly stable jet, zonally elongated and with two anticyclonic meanders East of Japan very intense (hereafter elongated state); and the other one much more convoluted and zonally

contracted (hereafter convoluted state). Shifting between the elongated state and the convoluted state the jet moves southward, the LKE and the EKE increase due to the dissipation of the two quasi-stationary anticyclonic meanders in much more eddies, interacting with each other, in an inverse energy cascade process. The shift in latitude is associated to the strengthening of the Aleutian Low, which enhances Sea Surface Height anomalies (SSHa) in the East-Central Pacific, that propagate westward as baroclinic Rossby wave trains (e.g. Latif et al., 1996; Mantua et al.,2002; Di Lorenzo et al., 2007; Qiu and Chen, 2010; Wu,2013).

The KE LFV has been characterized by several scalar indices in the past (e.g. Qiu and Chen 2005; 2010; Pierini, 2006; 2014). We used modeled and observed SSH fields, and surface geostrophic velocity (GSV) fields derived from SSH gradients and the coriolis parameter, to calculate four scalar indices characterizing the KE every 5 days: the KE velocity, the KE eddy kinetic energy (EKE), the KE Length (LKE), and the KE latitudinal position ($<\varphi>$).

The KE velocity index is calculated at every latitude between 30 and 40°N as the maximum amplitude of GSV integrated zonally in the Upstream KE region (141-153°E), where eddy-eddy interactions and the jet variability are strongest:

$$\mathrm{KE_{vel}} = \max|\mathrm{GSV}| \qquad (1)$$

EKE fields are deduced from GSV fields as

$$EKE = \frac{1}{2}\mathbf{u}' \cdot \mathbf{u}' \qquad (2)$$

where · is the scalar product and $\mathbf{u}'$ is the vector for the eddy component of the GSV field, defined as departures from the mean annual cycle. The EKE index is then obtained by averaging EKE over the region [141-153°E; 32-38°N].

<φ> and LKE indices are derived from the pathway of the Kuroshio axis in the Upstream KE region (141-153°E). The Kuroshio axis is defined as the SSH isoline where the meridional SSH gradient is maximum on average over this region; these isolines are SSH = 0.7 m in OCCIPUT simulations, and 0.9 m in the observations. <φ> and LKE indices are the latitude and length of the Kuroshio axis averaged zonally over the Upstream KE region.

These four scalar indices were computed for both model datasets and for the observations, then low-passed filtered using a LOWESS (Locally Weighted Scatterplot Smoothing) operator in order to focus on the KE interannual-to-decadal variability.

ii) The OCCICLIM pseudo ensemble

To perform a consistent comparison of the evolutions of these four scalar indices in OCCITENS and in OCCICLIM, we split the 300-year (ignoring the first 30 years of spinup) one-member OCCICLIM timeseries into fifty 36-year chunks, hence yielding a pseudo-ensemble having the same structure and size as the OCCITENS ensemble. Each of these 50 chunks starts on the first day (January 1st) of a random year of the original OCCICLIM timeseries, and therefore represents a 36-year realization of the pure intrinsic variability. The actual OCCITENS ensemble and the

OCCICLIM pseudo-ensemble are further processed and analyzed using the same approaches and tools, presented in the following.

The pure (quasi-autonomous) intrinsic variability of the Kuroshio will be characterized from the evolution of the four scalar indices in this OCCICLIM pseudo-ensemble, and compared to its atmospherically-modulated (non-autonomous) counterpart below. This comparison should help characterizing the role of the full atmospheric variability in exciting, damping, or pacing the pure intrinsic variability, using concepts of Dynamical Systems theory as done previously with much simpler numerical simulations.

iii) Non-linear detrending

Most geophysical timeseries include timescales that are longer than their actual length, which are likely to bias their analysis (e.g. variance or spectrum estimations). The same problem may arise when analyzing timeseries derived from primitive equation model simulations, which may contain long-term, possibly non-linear, spurious drifts due to mismatches between model initial states, forcing fields, and missing processes. We solve both possible issues in a way very similar to Leroux et al (2018), who used a LOESS detrending operator to remove both nonlinear trends and under-sampled low-frequency signals from their timeseries. Unlike these authors, we used an equivalent but more computationally-efficient LOWESS operator to achieve this goal. We finally applied the LOWESS operator (Burkey, J., 2013) on the following quantities: the four scalar indices introduced above for the actual OCCITENS ensemble (see Fig. 6), the OCCICLIM pseudo ensemble, and other fields shown in the figures of the present chapter (i.e. SSH and GSV

in OCCITENS). Besides its detrending effect, this operation suppresses exactly the same range of long timescales in the AVISO dataset, in the OCCICLIM pseudo-ensemble and in the OCCITENS ensemble.

iv) Estimating the intrinsic and forced variabilities

This section summarizes the first method (see Leroux et al, 2018 for more information) we used to analyze the OCCITENS dataset in terms of forced and intrinsic variabilities. Any pre-processed OCCIPUT-derived timeseries $f_i(t)$, i=1,N (either model outputs or any of the indices introduced above) in member i may be written as:

$$f_i(t) = \langle f(t) \rangle + f_i'(t) \tag{3}$$

where N is the number of members, the angled brackets denote the ensemble mean (an estimator of the atmospherically-forced signal) and the prime subscript denotes the intrinsic signal in member i. The total, forced and intrinsic variabilities (A_{total}, A_{forced}, $A_{intrinsic}$, respectively) may be estimated as:

$$\begin{cases} A_{total} = < \sigma_f > \\ A_{forced} = \sigma_{\langle f \rangle} \\ A_{intrinsic} = \sqrt{\overline{\varepsilon^2}} \end{cases} \tag{4}$$

where σ_f is the temporal standard deviation of timeseries f, ε^2 is the (time-varying) ensemble variance of the N f_i samples, and the overbar is the temporal averaging operator. It can be shown that $A^2_{total} = A^2_{forced} + A^2_{intrinsic}$. The amplitude ratio $R = \frac{A_{intrinsic}}{A_{forced}}$ is a simple estimate of the contribution of intrinsic processes to the total variance of signal f. Note that the same

statistics may be applied on the OCCICLIM pseudo-ensemble, where by construction the interannual-to-decadal variability is purely intrinsic (and quantified by $A_{intrinsic}$) and the forced variability A_{forced} close to zero.

The left panels in Fig.6 show for the four scalar indices derived from OCCITENS the forced signals (black lines), the ensemble standard deviation σ (half-width of the blue band), and the amplitude ratio R. The forced variability exceeds the intrinsic variability ($A_{forced} > A_{intrinsic}$) only for $<\varphi>$ with R=0.6: the interannual-to-decadal variability of the mean latitudinal position of the Kuroshio is mostly atmospherically-driven, despite a significant contribution of the intrinsic variability. In contrast, the interannual-to-decadal variability of LKE, KE_{vel} and EKE are dominantly intrinsic (R=2.82, 2 and 2.6 respectively), indicating that the atmospheric variability is only a secondary driver of these Kuroshio features. This is in agreement with the theory suggested in Pierini (2014), who interpreted the KE LFV as a case of intrinsic variability paced by an external forcing.

This first method assumes that the oceanic variability in an ensemble like OCCITENS may be separated into both components, and fully described using the first and second moments of the random variable $f_i(t)$.

This is possible in simple cases: the time-varying ensemble average (forced signal) and variance (intrinsic variability) fully describe the time-varying ensemble PDF if the latter remains Gaussian. This simple method may also be used to describe the main features of random variables whose time-varying PDFs are close to Gaussian, or at least symmetric. Figs. 6 and 7 show that the time-varying ensemble PDFs of the four scalar indices approximately fall into this category, and hence be analyzed as presented above, at least preliminarly.

However, if the time-varying ensemble PDF of a variable is non-Gaussian (as may be expected in the KE, see the introduction), this simple description of the variability remains uncomplete, and its separation into forced and intrinsic components potentially irrelevant. In such cases, concepts and techniques derived from the theory of non-autonomous Dynamical Systems may provide more insightful and mathematically-grounded descriptions of the system behavior. We will propose in section 3 an attempt in that direction, with additional diagnostics inspired from such theories.

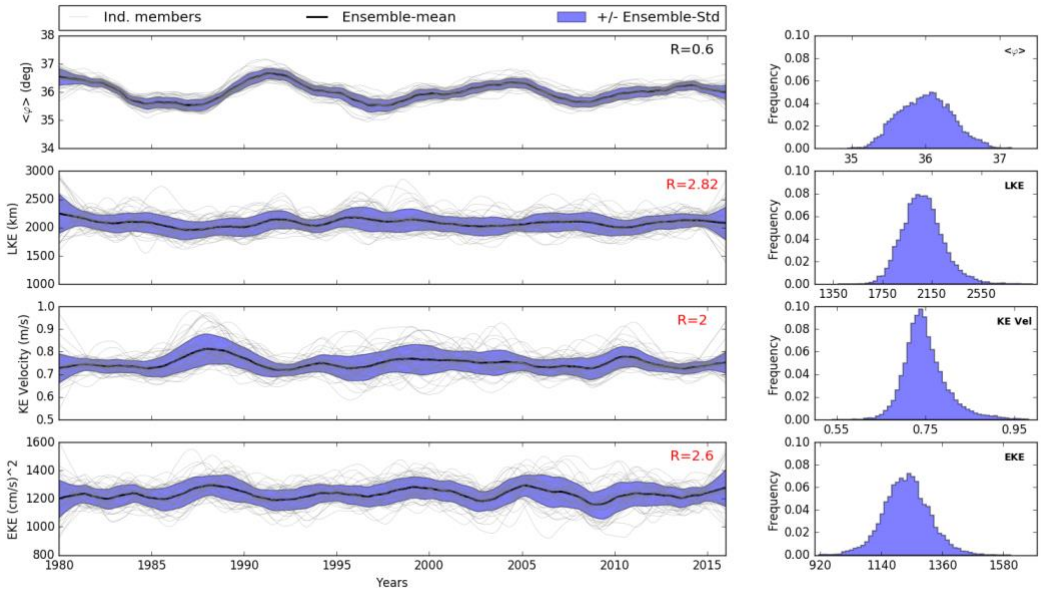

Fig.6. (Left) Time series of the low pass filtered indices (mean latitudinal position, LKE, KE velocity, EKE) from ENSx50- occi025 after nonlinear (LOWESS) detrending. The 50 individual trajectories are shown with the thin gray lines; the ensemble mean is shown with the thick black line; and the ensemble standard deviation is shaded. (Right) Climatological PDF of the low pass filtered indices (mean latitudinal position, LKE, KE velocity, EKE). R indicates the amplitude ratio.

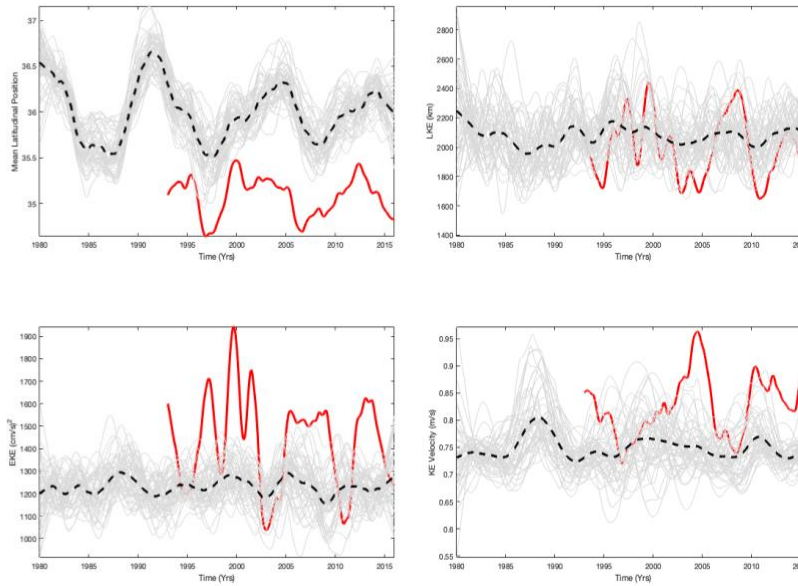

Fig.7. Time series of the low pass filtered indices (mean latitudinal position, LKE, EKE, KE Velocity) from ENSx50- occi025 after nonlinear (LOWESS) detrending. The 50 individual trajectories are shown with the thin gray lines; the ensemble mean is shown with the shaded black line; in red the time series of the low pass filtered indices (mean latitudinal position, LKE, EKE, KE Velocity) from AVISO.

2.2.3 Assessment of the KE LFV in OCCITENS

The KE LFV in OCCITENS is now assessed by comparing the 50-member evolution of the four scalar indices with the evolution of their observed counterpart (see Fig. 7). As explained in the previous section, each ensemble member represents a superposition of a common variability (the forced variability given by the ensemble mean) and a random intrinsic variability (deviations from the ensemble mean). As explained in Leroux et

al. (2018), the observed variability may be seen as a single realization of the real ocean evolution, and is very likely to include a random component that is out of phase with any of its simulated realizations.

Evaluated against the observations, the latitudinal position of the KE appears to be shifted to the north by about 1° in all OCCITENS members; this overshoot of western boundary currents is typical of eddy-permitting simulations, and had been already noted in a previous 1/4° global NEMO simulation (Penduff et al, 2010). However this bias does not hinder the study of the variability itself. As noted above, the interannual-to-decadal fluctuations of the jet latitude are predominantly controlled by the atmospheric variability: the ensemble mean $<\varphi>$ clearly exhibits forced fluctuations, which reflect the atmospherically-forced part of the observed signal. This impact of the forcing on the low-frequency KE latitude may be mediated by the propagation of long Rossby waves across the Pacific (e.g. Qiu and Chen, 2005, 2010).

The typical length (LKE ~2200km) of the observed KE is well simulated in the model, but its typical EKE and velocity are smaller than observed as expected in any eddy-permitting simulation (other panels of Fig. 7). The interannual-to-decadal variability of these three indices was shown to be mostly intrinsic, as confirmed by their large random dispersion around the ensemble mean. The intrinsic nature of LKE and EKE fluctuations may be due to the large imprint of the random eddy field on these indices. The KE_{vel} variability is expected to be sensitive to the eddy field too (through e.g. rectification; Nonaka et al.,2012), but is slightly more sensitive to the forcing variability, presumably because it is related more directly to the jet's latitudinal shifts (as shown in section 2.3).

The realism of the OCCITENS ensemble simulation is now assessed against the observed interannual-to-decadal variability of the four KE indices, over the common available period (1993–2015). Results are summarized in Fig. 8 as Taylor diagrams (Taylor, 2001), which exhibit the temporal correlation coefficients, STD ratios and RMS errors between each modeled timeseries and their AVISO counterparts. The correlation coefficients between the KE mean latitude $<\varphi>$ in each member and the observations span a very large range (0.1-0.8), and reach the largest values in members where the intrinsic variability phase happens to better match the observational reference. The $<\varphi>$ STD ratio exhibits a large inter-member diversity as well (0.7-1.6), but the simulated $<\varphi>$ variability averaged over the 50 members is close to the observational estimate. This large span between members illustrates the strong dependence of model-observation comparisons on a particular intrinsic variability realization, and demonstrates the poor robustness of such a comparison when only one eddying model integration is available. As the ensemble averaging operator suppresses the intrinsic "noise" from simulated timeseries, the ensemble mean timeseries exhibits a smaller STD ratio (and a larger correlation with the observations) than any of the individual members.

The fluctuations of the KE velocity and length reach about 70% of their observed amplitude on average over the ensemble, but with a rather large inter-member scatter due to the larger contribution of intrinsic processes to these indices' variabilities. The strongly intrinsic (hence random) character of these simulated (and presumably observed) quantities explains the small simulation-observation correlations found in each member, and the small STD ratio and correlation of their ensemble mean with the observations.

The cloud of points clearly shrinks toward the origin for the EKE interannual-to-decadal variability, as the model only represents about 40% of its observed magnitude.

To summarize, these Taylor diagrams provide a rather precise view of the interannual-to-decadal KE variability in the OCCITENS ensemble, and highlight the importance of intrinsic, random fluctuations of the system. The model correctly simulates the deterministic part of the interannual-to-decadal variability of the KE latitude, with a general tendency to underestimate the eddy variability.

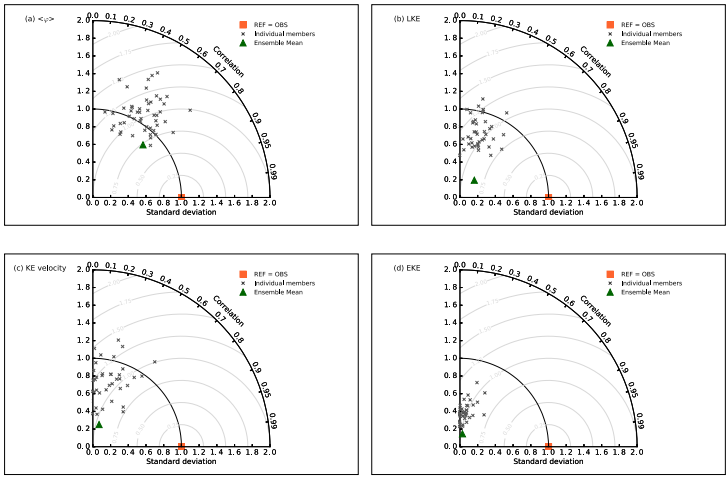

Fig.8. Taylor diagram (Taylor 2001) using the 1993–2017 AVISO observational time series (LPF) as the reference. The AVISO time series is compared to the LPF (mean latitudinal position (a), LKE (b), KE velocity (c), EKE (d) time series of each ENSx50-occi025 individual member and to the ensemble-mean time series. For each point on the diagram, the angle with the horizontal axis shows the correlation with the reference time series, and the radial distance to the origin shows the ratio of their time standard deviations. In addition, the radial distance to the reference point (orange square) corresponds to the RMS between the two timeseries.

2.3 The KE LFV: intrinsic versus forced mechanisms

The gaussian metrics applied to the KE indices mentioned in the previous section show that both the intrinsic and forced variabilities contribute to the total variability of the system; in particular, the external forcings excite the broad-scale variability more than the frontal one which is dominated by the intrinsic oceanic mechanisms. To highlight the atmospherically forced variability we examine in Fig.9 the Ensemble Mean Hovmöller Diagram for the SSHa in the longitude-time domain (looking at both the upstream and downstream regions), in comparison with the LKE-ensemble mean-anomaly (LKEa), defined as the departure from the mean value, and the SSHa timeseries computed for every member in the PDO center of action (175-180°W). Fig.9 suggests that there is a teleconnection mechanism provided by baroclinic Rossby wave trains, which link perturbations in the SSHa in the East-Central Pacific (175-180°W) and in the Upstream KE region. The anomalies are here computed for every member as the departure from the climatological mean field and averaged between 32-34°N as Qiu and Chen (2010), the ensemble mean is then computed for each grid point. The SSH anomalies move westward from the PDO center of action which is located in the east-central Pacific, pacing the KE variability. The signal excited from the atmosphere between 175-180°W is coherent between the members, which are in phase. A higher LKE in the ensemble mean corresponds to positive SSHa, which excite the shift from the elongated state to the convoluted state in an atmosphere-driven regime. In contrast, by adding oceanic noise the link between the external forcing and the two states lose coherence due to the contribution of the internal variability.

Similar features are shown by Fig.10, which presents a comparison between the Hovmöller Diagrams of the SSHa of AVISO, of a single OCCITENS member and of the ensemble mean in the latitude-time domain averaged in the Upstream KE region. The figure clearly shows that the latitudinal shift of the jet (highlighted by the presence of the two quasi-stationary anticyclonic meanders) is atmospheric driven since it is captured by the ensemble mean, but the total KE variability is modified by internal mechanism, which, through eddy formation and eddy interaction enhance the chaoticity of the oceanic system by modulating the LFV of the jet. Shifting from the elongated to the convoluted state, the jet moves southward, while the two quasi-stationary anticyclonic circulations in the KE are dissipated through energy conversion processes (Yang and Liang, 2016) and an equatorward eddies propagation. This mechanism is captured both by the ensemble mean and the ensemble members, but the oceanic chaos enhances even more their propagation (Fig.10).

This analysis has been applied also at the GSV field for AVISO, for the Ensemble Mean and for one single member of OCCITENS. Fig.11 confirms that the latitudinal shift of the jet from quasi-decadal to decadal timescales is atmospheric driven (as evinced by the position of the maximum of GSV). Compared to the ensemble mean, the amplitude of the GSV is doubled in the full-variability field (AVISO and the OCCITENS members), suggesting that the introduction of noise in the oceanic system leads to a stronger jet with an increased EKE and available potential energy. In fact, many more eddies are captured by the full-variability field, so that the intrinsic oceanic variability drives the formation of vortices in the KE region: their variability is paced by the external forcing, but it is modified by internal mechanisms.

When introducing the oceanic noise, the GSV variability is much higher, as already observed in Fig.8.

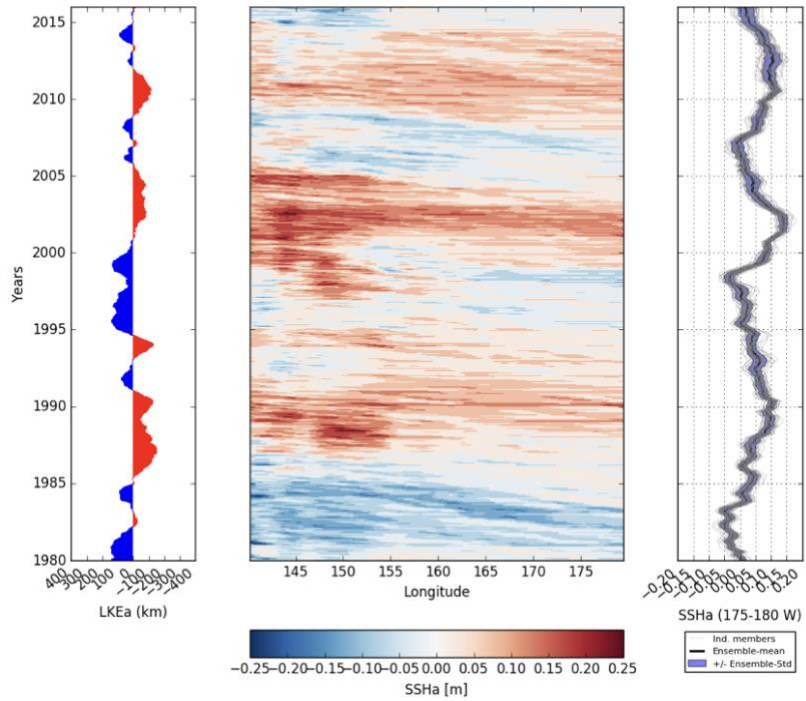

Fig.9. Left) LKE anomaly for the ensemble mean (negative values in red, positive values in blue). Center) Hovmöller diagram for the SSHa computed for the ensemble mean (averaged between 32-34°N). Right) Time series of the low pass filtered SSHa (averaged between 32-34°N;175-180°W) from ENSx50- occi025 after nonlinear (LOWESS) detrending. The 50 individual trajectories are shown with the thin gray lines; the ensemble mean is shown with the thick black line; and the ensemble standard deviation is shaded.

These results suggest that both the intrinsic and forced variabilities contribute to the total KE LFV; therefore, to define the role played by the external forcings in the KE dynamics, we take advantage of the climatological run OCCICLIM, which provides the KE pure-intrinsic variability. By comparing OCCITENS with OCCICLIM we will be able to better define the role of the external forcing. Since the climatological run is a 330 yrs one-member realization, we created a pseudo-ensemble from OCCICLIM, made of 50 members, 36 years long each. Since aperiodically forced systems are nonergodic (Drotos et al., 2016), the ensemble thus obtained cannot be considered as equivalent to an ensemble simulation in which the members differ by their initialization (as in OCCITENS); it will, nonetheless, turn out to be very useful in the following discussion.

This strategy evaluates the pure-intrinsic variability in the KE system and the role of the external forcings in exciting, modulating, damping, or pacing intrinsic modes of oceanic variability that are identified from the OCCICLIM climatological simulation.

2.3.1 An autonomous dynamical system: the KE pure intrinsic variability in OCCICLIM

As already discussed in section 2.2, the KE indices are found to be interdependent. In the elongated state the jet is located more northward, the LKE and the EKE are lower, whereas in the convoluted state the jet shifts southward and the LKE and EKE increase. Fig.11 also highlights the link between the KE_{vel}, which well identifies the LFV of the jet on decadal time scales, and the mean latitudinal position of the jet. Since the broad-scale variability of the jet is captured by the $<\varphi>$ index and the frontal-scale

variability is captured by the LKE, the EKE and the KE_{vel}, in order to merge these information, we compute the Joint Probability Distribution (JPD) in the two-dimensional phase-space Φ-Ψ, with Φ given by the KE mean latitudinal position and Ψ provided by LKE, EKE or KE_{vel}. This approach helps to identify what are the main clusters populated by the system taking into account both the broad-scale variability (which is mainly atmospheric driven) and the frontal-scale variability (which is mainly led by internal mechanisms). This statistical diagnostic computes the likelihood of two events occurring together, providing the distribution of the clusters visited by the KE and the attractor in the Φ-Ψ state space. Since the KE indices are not independent, we expect the same attractor even changing the Ψ variable. A preliminary step has been done to confirm this expectation (not discussed in this chapter) plotting the JPD for the three available Φ-Ψ combinations; the attractor is assessed to be the same in every phase-space. For simplicity we will show only the JPD in the Φ-KE_{vel} domain.

First, we computed the JPD for the autonomous dynamical system, by taking advantage of the pseudo-ensemble built with OCCICLIM. This provides the KE attractor without any contribution of external forcing. By merging the members for every year, we computed the JPD in the Φ-Ψ domain, building a timeseries of the JPD (see additional material). The bimodality of the KE LFV is captured by the JPDs: two are more populated by the jet, whose share the same Ψ range of values, but are displaced along the latitudinal position (Fig.12). One peak is located at higher latitudes (~37-38°N), another is located more southward (~ 35.5-36.5 °N). Fig.12 displays also the position of the center of gravity, which moves between three locations along the 36-yrs timeseries: two of them represent the two modes,

with the transition phase in the middle. According to the dynamical systems theory increasing the number of data the attractor explores the phase-space moving always in the same region through several trajectories time-dependent. Therefore, whatever is the isoline that we take as reference to look at the attractor's area in the phase-space, we expect that the extension of the region explored by the system is constant in time. In contrast, in our case the ratio (in percentage) between the maximum area explored by the 10% isoline along the whole timeseries and the 10% instantaneous isoline for every timestep converges to 100% but it varies in time around this value (Fig.13). We suggest that this mismatch with the dynamical systems theory is due to the lack of data and therefore increasing the number of members this ratio would fit the expectations.

These results consistent with the assumption suggest that the bimodality of the jet is purely intrinsic, but no information is provided about the action of the external forcing in shaping the KE LFV: this can be extracted by the analysis of the OCCITENS dataset, which includes both the intrinsic and external variability of the system.

2.3.2 A nonautonomous dynamical system: OCCITENS

Where the JPD applied to the OCCICLIM dataset provides the attractor in an autonomous dynamical system, the same methodology applied to the OCCITENS data provides the attractor of a nonautonomous dynamical system. These diagnostics highlight the main clusters populated by the KE along the 36-yrs timeseries. The JPD spans several states, the main ones being diagonally located: one yields lower latitudes and higher KE_{vel} (~35°N; ~0.7÷0.8 m/s) and the other one shifted more northward and with lower

KE_{vel} (~36.5°N; ~0.6÷0.7 m/s). The KE oscillates in the phase space much faster in the nonautonomous system (Fig.14; Fig.15); the center of gravity loop (Fig.15) shows the locations occupied by the jet in the attractor. Along the 36-yrs time series, sixteen positions are identified. Two loops are shown by Fig.15: a wide one turning clockwise and a more restricted one anticlockwise. The opposite phases of the orbits indicate that there is not a prior direction in the shift between the two main states through the transition phase. Fig. 16 shows the ratio between the area explored by the 10% instantaneous isoline at every timestep and the maximum area explored by the 10% JPD for OCCITENS: this figure differs from Fig.13 because in this framework the ratio gives a measure of the action of the external forcings on the KE variability: the higher is the ratio, the lower is the action of the external forcings. How the atmosphere acts on the internal variability is analyzed in the next section by comparing the results from OCCICLIM and OCCITENS, that differ only by the presence of the forced variability in the OCCITENS dataset.

2.3.3 Intrinsic variability paced by external forcings

The creation of the pseudo-ensemble for OCCICLIM helps answering to the following question: - What is the role of the intrinsic mechanisms and external forcings in the KE LFV?

In fact, the JPDs provide a clear footprint of the attractor in the autonomous and nonautonomous dynamical systems. The differences between the JPDs can reveal the role played by the external forcing.

Fig.17 shows the climatological JPDs in the two systems and helps to define the role of the atmosphere in the KE LFV. With the introduction of the external forcings the system explores a more restricted region of the phase-space; moreover, the two modes are tilted clockwise and diagonally distributed. Therefore, the external forcing reduces the size of the attractor. The KE oscillates between the two quasi-stationary states crossing one transition point in the autonomous system only; on the other hand, under the external forcings the jet moves from the elongated to the convoluted state following a clockwise or counterclockwise rotation.

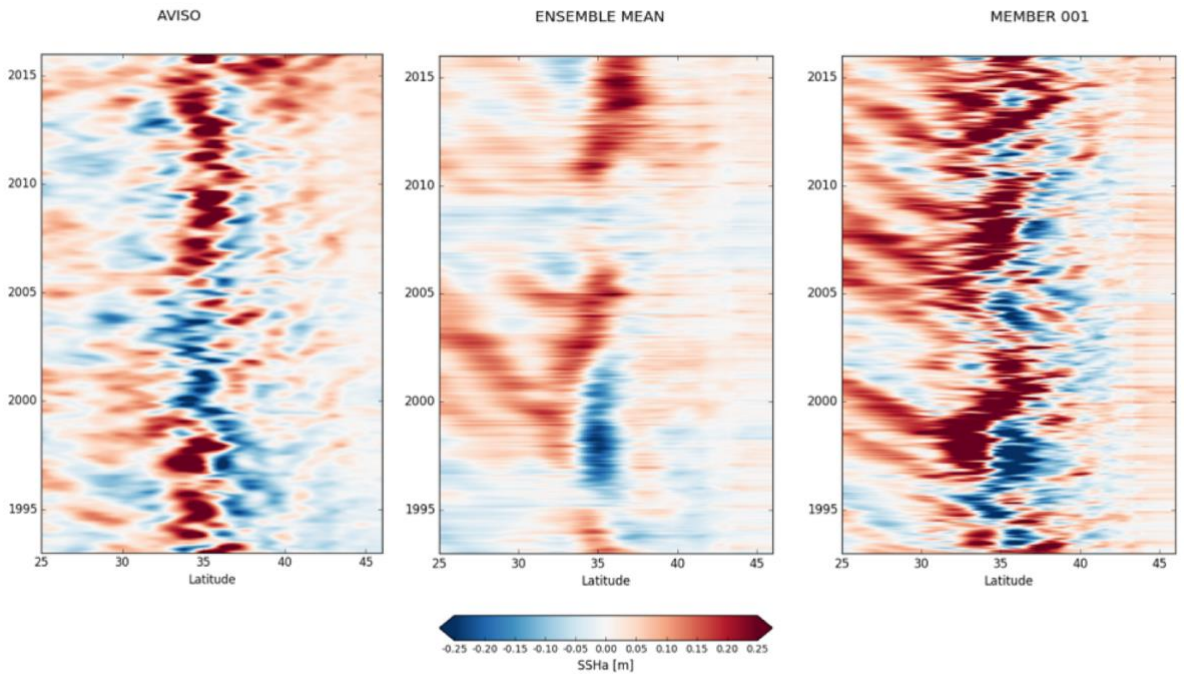

Fig.10. Hovmöller diagram for the SSHa in the latitude-time domain (averaged in the upstream KE region) for AVISO (left), the ensemble mean (center) and one ensemble member (right).

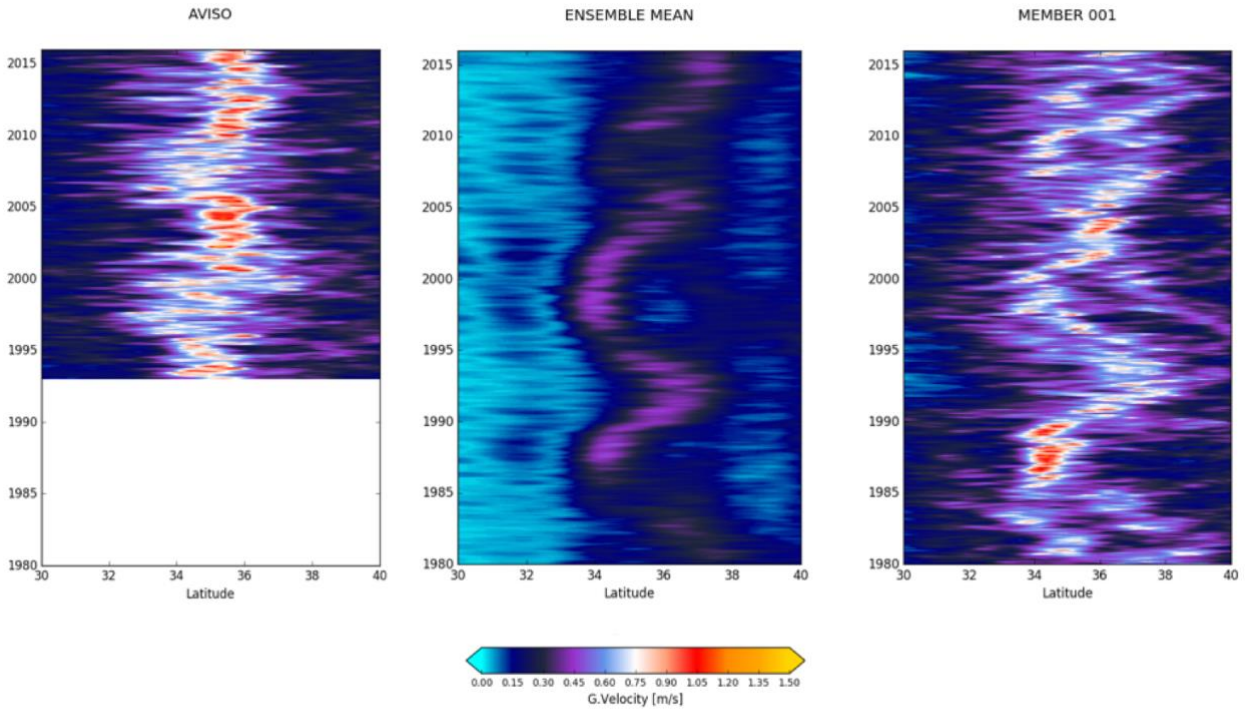

Fig.11. Hovmöller diagram for the GSV field in the latitude-time domain (averaged in the upstream KE region) for AVISO (left), the ensemble mean (center) and one ensemble member (right).

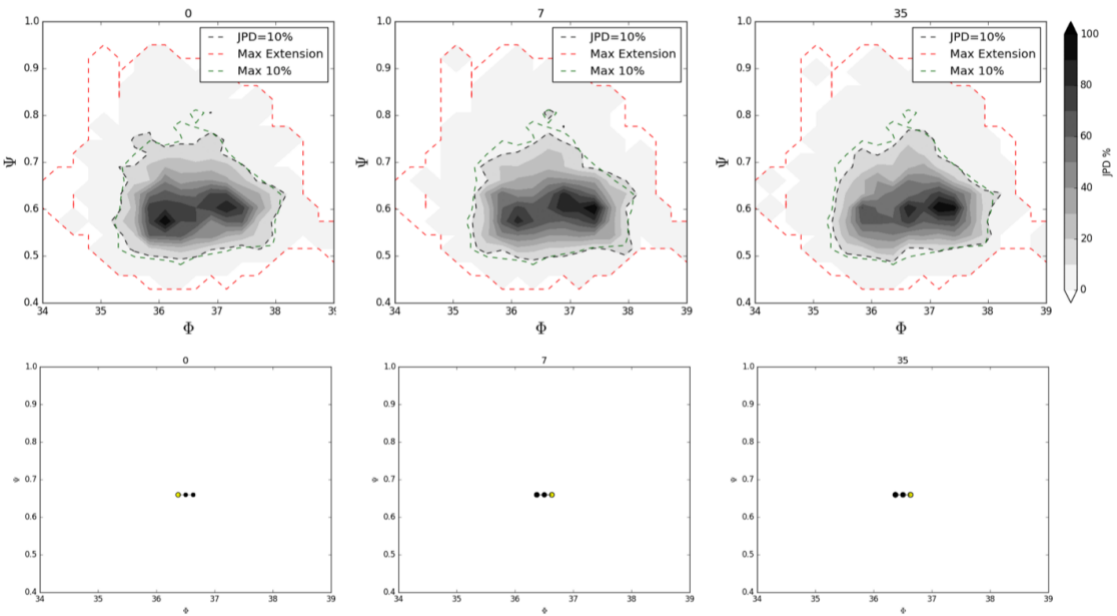

Fig.12. Top) The yearly JPD in the mean latitudinal position (Φ) - KE velocity (Ψ) domain for the years 0,7 and 35 in the OCCICLIM pseudo-ensemble. The shaded lines are the 10% instantaneous JPD (black), the maximum 10% JPD isoline extension along the 36-yrs time series (green) and the maximum extension of the 0% JPD isoline along the 36-yrs time series (red). Bottom) The center of gravity positions of the JPD for each year (yellow dot) and along the 36-yrs time series (black dots).

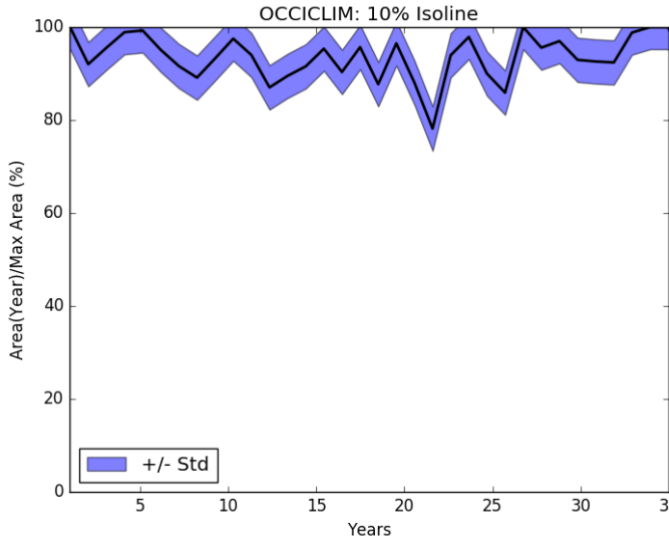

Fig.13. Ratio between the area of the instantaneous 10 % isoline and the maximum area explored by the 10 % isoline along the 36-yrs time series in the OCCICLIM pseudo-ensemble.

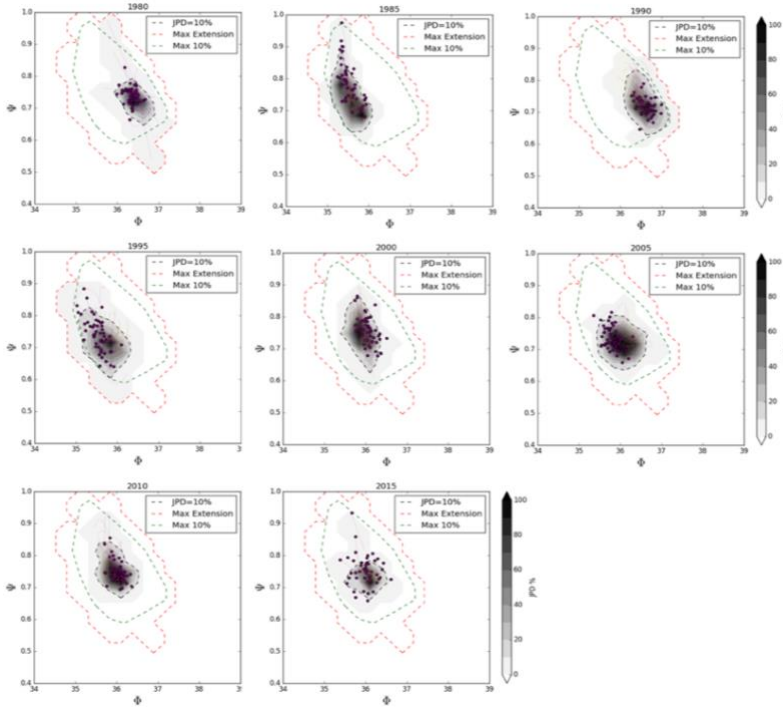

Fig.14. The yearly JPD in the mean latitudinal position (Φ) - KE velocity (Ψ) domain every 5 years between 1980-2017 in the OCCITENS ensemble. The shaded lines are the 10% instantaneous JPD (black), the maximum 10% JPD isoline extension along the 36-yrs time series (green) and the maximum extension of the 0% JPD isoline along the 36-yrs time series (red). The purple dots are the last points (Φ-Ψ) of the trajectories (thin purple lines) for every member at each year.

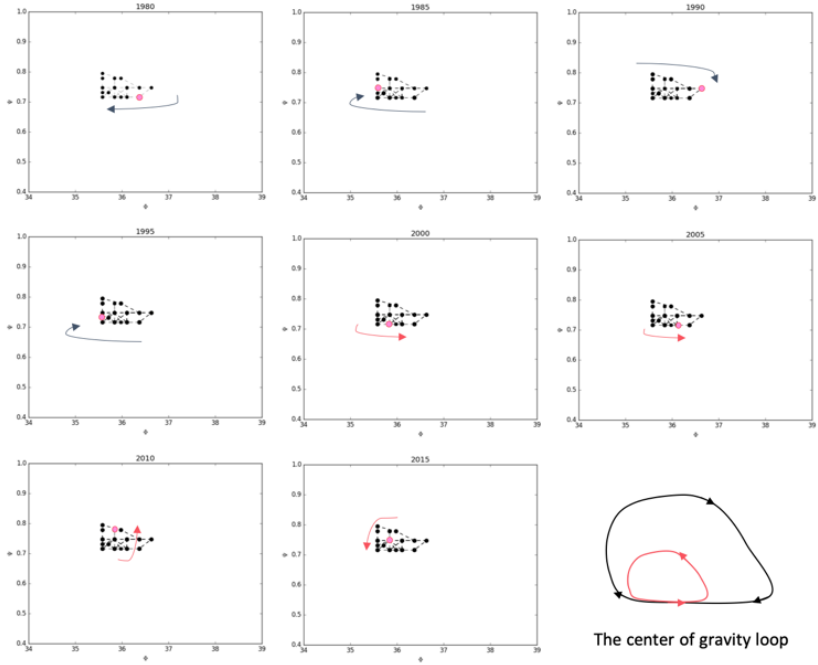

Fig.15. The center of gravity positions of the JPD for each year (pink dot) in the mean latitudinal position (Φ) - KE velocity (Ψ) domain every 5 years between 1980-2017 in the OCCITENS ensemble. The last bottom panel shows a sketch of the center of gravity loop along the 36-yrs time series.

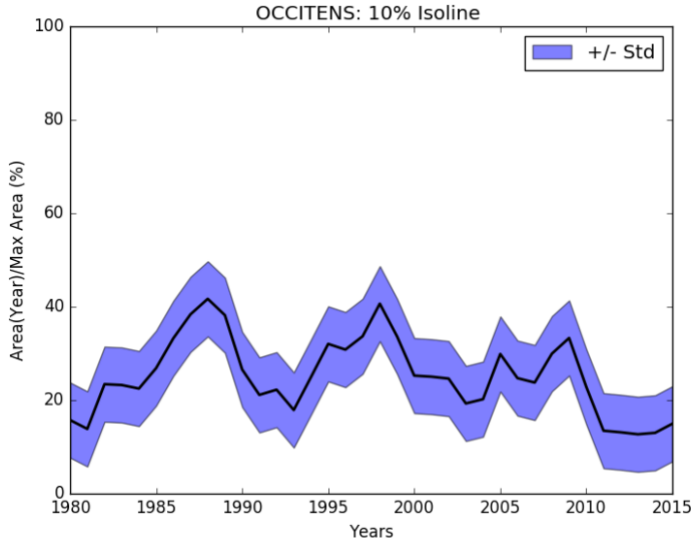

Fig.16. Ratio between the area of the instantaneous 10 % isoline and the maximum area explored by the 10 % isoline along the 36-yrs time series in the OCCITENS ensemble.

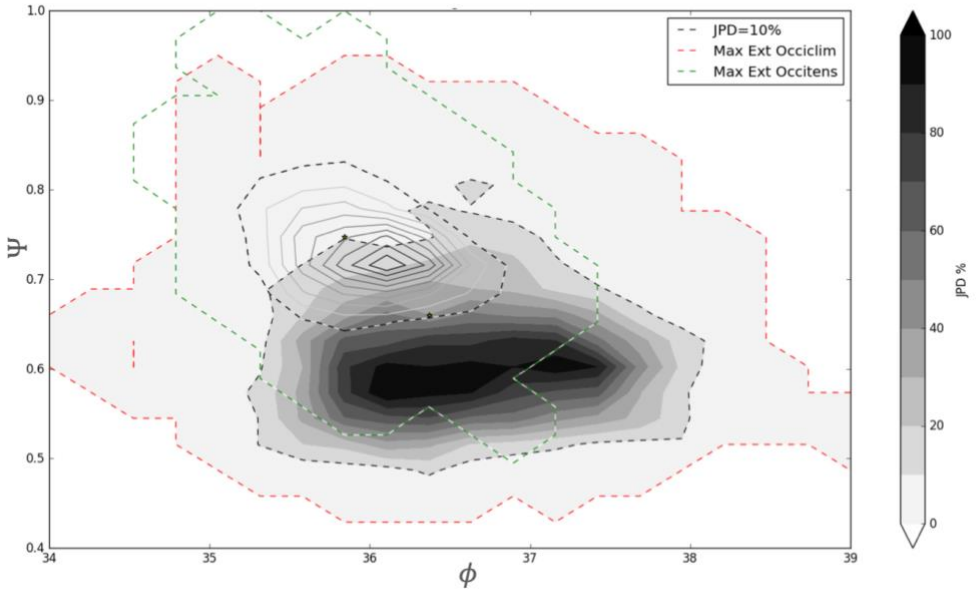

Fig.17. The Climatological JPD in the mean latitudinal position (Φ) - KE velocity (Ψ) domain for the time series: 1980-2017 in the OCCITENS ensemble (contours) and in the OCCICLIM pseudo-ensemble (filled contours). The shaded lines are the 10% instantaneous JPD (black), the maximum 0% JPD isoline extension in OCCITENS along the 36-yrs time series (green) and the maximum extension of the 0% JPD isoline along the 36-yrs time series in OCCICLIM (red).

2.4 Conclusions

This work has been devoted to the analysis of the KE LFV nature, which is still under debate and poorly understood. Our main findings make a step forward in the comprehension of this phenomenon; taking advantage of the ensemble techniques and investigating the interannual -to- decadal variability of the jet from the dynamic systems theory viewpoint, in this study we show that the KE LFV is an internal oceanic variability paced by external forcings. The bimodality of the jet is well captured by an autonomous system (OCCICLIM), strongly supporting that it is driven by intrinsic mechanisms, while the nonautonomous system (OCCITENS) is also able to capture the KE LFV but the attractor looks different due to the action of external forcings. In this framework, the two main equilibrium points are rotated in a phase-space that is smaller compared to the phase-space explored in the autonomous case. The atmosphere acts reducing the region of the phase space explored by the KE dynamical system. Without external forcings the system oscillates slowly between two quasi-stationary states, while introducing the atmospheric contribution the KE jet explores the phase-space following many orbits with a low persistence and without a prior direction.

The oceanic intrinsic variability drives the KE LFV, which is therefore defined as an oceanic-driven mechanism, where the eddies-interaction play a fundamental role. In this context, to increase the oceanic resolution of the ensemble simulations moving from an eddy-permitting regime (OCCIPUT like) to an eddy-resolving regime could provide many improvements in the degree of realism of the KE. Moreover, in an eddy-resolving configuration

we could explore the internal oceanic mechanisms, with a better understanding of the processes that lead the LFV of the jet.

Other improvements can also be introduced having a larger number of ensemble members. As suggested in section 2.3.1, adding members in the climatological run, the results would fit better the dynamical systems theory.

Chapter 3

Decadal variability of the Kuroshio Extension: The response of the jet to increased atmospheric resolution in a coupled ocean-atmosphere model

3.1 Introduction

The Kuroshio Extension (KE) is the eastward meandering jet formed by the convergence of the Kuroshio and Oyashio western boundary currents in the Northern Pacific Ocean. The KE is known for exhibiting low frequency variability (LFV) over interannual and decadal time scales; the jet shifts between two main states, one fairly stable and zonally elongated (hereafter elongated state) and the other one highly variable and convoluted with a reduced zonal penetration (hereafter convoluted state).

Regarding the mechanisms underlying the KE LFV, two schools of thought with conflicting views exist. The debate revolves on the relative roles of intrinsic variability and external forcing in driving the quasi-decadal variability of the jet. The first view supports the idea that the KE LFV is an intrinsic mechanism led by the nonlinear interaction of recirculation, potential vorticity advection and eddies (e.g. Jiang et al., 1995 and Dijkstra and Ghil, 2005; Pierini, 2006). Several studies (Schmeits & Dijkstra, 2001; Dijkstra and Ghil, 2005; Pierini, 2006) show that the two regimes can be reproduced using simple double-gyre idealized models forced with steady-state winds, in agreement with altimetry data (Qiu, 2003; Qiu and Chen, 2005; 2010). These studies interpret the mechanism which leads the shift from the elongated state to the convoluted one as linked to the eastward

propagation of potential vorticity anomalies from the western boundary current region (Cessi et al., 1987).

In contrast, the second view supports that the KE LFV is induced by broad-scale atmospheric patterns of variability such as the Pacific Decadal Oscillation-PDO (e.g., Miller et al. 1998; Deser et al. 1999; Qiu 2003; Qiu and Chen 2005). To support this theory, Taguchi et al. (2007) have confirmed through an eddy-resolving ocean general circulation model (OGCM), that the KE LFV is synchronized with large-scale atmospheric variability via the propagation of Rossby waves from the East-Central Norther Pacific. In this context, it has also been shown that the frontal-scale variability contributes to changes in the KE jet speed, which can be generated by intrinsic oceanic mechanisms, highlighting that while the linear Rossby wave theory explains the temporal variability, nonlinear ocean dynamics plays an essential role in organizing the spatial structure (Taguchi et al., 2007; Nonaka et al., 2012). To support the theory where both the intrinsic and forced components play a role in the KE LFV, Pierini (2014) showed that the KE decadal bimodal cycle can be interpreted as a case of intrinsic variability paced by an external forcing in an ocean circulation model of the North Pacific forced by climatological winds perturbed with the North Pacific Oscillation forcing. Both viewpoints agree that the intrinsic oceanic variability plays a fundamental role in the KE LFV.

In order to better clarify the relative roles of internal and externally induced variability on the KE LFV, it is important to rely on realistic models of the ocean-atmosphere coupled system. Ma et al. (2016; 2016b) analyze the effect of air–sea coupling on the KE by comparing atmosphere–ocean coupled models at different resolutions. These results point to the relevance

of explicitly resolving oceanic mesoscale eddies in order to faithfully reproduce the dynamics of, and the factors controlling, the KE jet. While it is clear the importance of the spatial resolution in the oceanic component through the representation of ocean mesoscale turbulence and relative interaction with the atmosphere, the impact of the horizontal resolution of the atmospheric component on the main features of the KE jet and on its variability on quasi-decadal timescales has been relatively less inspected (e.g. Sakamoto et al., 2012; Delworth et al., 2012; Small et al., 2014).,

In this work we analyze the output of a fully coupled GCM, run under the HighResMIP experimental protocol (Haarsma et al., 2016), specifically designed to inspect the effect of resolution on several key processes of the climate system. The specific goal of our analysis is to investigate the impact of model resolution on the representation of KE LFV, that we analyze both in terms of frontal-scale and broad-scale variability, making a step forward into assessing the role of the horizontal atmospheric resolution on the degree of realism of the KE jet.

In this context, by using different resolutions in coupled model configurations from the CMIP3 and CMIP5 archive (see section 3.2.1), many authors inspect their role (both in the ocean and atmospheric components) on several processes such as aspects of the large-scale circulation, small-scale phenomena, extreme events, upwelling, oceanic eddies, SST fronts, boundary currents and coastal currents (e.g. Sakamoto et al., 2012; Delworth et al., 2012; Small et al., 2014; Haarsma et al., 2016). Among them the mean features of the KE have been analyzed by focusing on the LFV of the jet but only with reference to its climatology.

In this context, Sakamoto et al. (2012) noticed significant improvements in the degree of realism of the KE jet if the horizontal atmospheric resolution is increased in two coupled configurations: MIROC3m and MIROC3h, leaving the oceanic resolution unchanged. In MIROC3m, the horizontal resolution is 2.8125° for the atmospheric component, while in MIROC3h it is 1.125°. These configurations share the same resolution for the ocean component: 1.40625° (zonal) × 0.56°–1.4° (meridional). In this framework they observe that a finer horizontal resolution in the atmosphere introduces improvements in the orographic winds and on their effects on the ocean; but what would happen with an even finer horizontal atmospheric resolution?

It is not obvious that increasing the resolution has always benefits on the degree of realism of the phenomena. In this context, Vannière et al. (2019) showed that one cannot necessarily expect that all features of the simulated climate be more accurate or in better agreement with the observations at higher resolution.

Therefore, we extend this study to the recent outputs from the High-Resolution Model Intercomparison Project (HighResMIP) for CMIP6 with an eddy-permitting ocean component and higher horizontal atmospheric resolutions (section 3.2.1). We not only investigate the effect of the atmospheric resolution on the oceanic mean field but in addition we look at its impact on the KE LFV, which has never been done before.

Being able to evaluate the benefits of advanced and well-evaluated high-resolution global climate models, compared to model at lower resolution on the KE dynamical system, is fundamental for tuning the next model

generations in order to define the best configuration able to simulate and predict regional climate with unprecedented fidelity.

This chapter is organized as follows. In section 3.2, we describe the dataset and methods used in this work referring both to the observations and models. In section 3.3 we show: (i) the impact of the horizontal resolution of the atmospheric model on the KE dynamical system (both in terms of mean field and LFV), (ii) the influence of large-scale ocean-atmosphere variability on the jet and (iii) the effect of the horizontal resolution of the atmospheric model on the air-sea interaction. In section 3.4 some conclusions are proposed.

3.2 Data and methods

3.2.1 Models and experimental setup

The model configurations used in this work are the Centro Euro-Mediterraneo sui Cambiamenti Climatici (CMCC) coupled atmosphere–ocean general circulation model CMCC-CM2-HR4 (High Resolution, HR) and CMCC-CM2-VHR4 (Very-High Resolution, VHR), which are in turn part of the wider CMCC-CM2 family of models, documented in Cherchi et al. (2018). The HR and VHR configurations have been implemented and developed in the framework of the H2020 PRIMAVERA project (https://www.primavera-h2020.eu), following the High Resolution Model Intercomparison Project (HighResMIP) for CMIP6. These are composed of version 4 of the Community Atmosphere Model (CAM; Neale et al 2013), NEMO3.6 for the ocean (Madec, 2016), CICE4.0 for sea ice (Hunke et al., 2015), and version 4.5 of the Community Land Model (CLM, Oleson et al 2013). Both HR and VHR configurations share the same eddy-permitting

ocean resolution (ORCA025, i.e. 0.25 degrees). The standard resolution configuration (HR) has a resolution of 1 degree in the atmosphere (64 km at 50°N), while the enhanced resolution (VHR) configuration has a resolution of 0.25 degree (18 km at 50°N) (see Table 2 for a summary of the models' characteristics).

Two 100-year control simulations of the present climate are conducted using fixed 1950s forcing conditions (referred to as "control-1950" in HighResMIP; Haarsma et al., 2016). These simulations are the present climate equivalent of the CMIP6 DECK preindustrial runs (Eyring et al., 2016). Since external forcings are time invariant, only the intrinsic variability of the coupled system is represented (i.e., no trends associated with observed changes in GHG concentrations, aerosol loadings, ozone and land use are included).

This set of model simulations provides an optimal framework to explore the sensitivity of the KE dynamics and its low frequency variability to changes in the model resolution. In the following analyses daily and monthly mean outputs of SSH and ocean current velocities are used.

3.2.2 Observational data

For SSH, daily data on a 0.25-degree grid from the AVISO dataset (Archiving, Validation, and Interpretation of Satellite Oceanographic data; see AVISO webpage, http://www.aviso.altimetry.fr, and the User Handbook) for the 1993-2017 period have been exploited. Gridded multi-satellite geostrophic velocity (GSV) data, derived from Maps of Absolute

Dynamic Topography (MADT), also provided by AVISO, were used to diagnose the surface flow pattern and the EKE field.

For SSTs, 1° monthly mean fields from the HadISST dataset (Rayner et al. 2003) have been used to diagnose the PDO index from 1871 to the present. This dataset provides a perfect framework to capture climate patterns of variability since the timeseries is long enough to give robustness to the analysis.

Finally, the ¼° daily SSTs from the NOAA OISST product (Reynolds et al. 2007) for years 1985–2013, combined with 1°, daily latent and sensible heat fluxes from the Woods Hole Oceanographic Institution objectively analyzed air–sea fluxes (OAFlux; Yu et al., 2008) were used to compute covariance maps and correlations between SST and surface turbulent heat fluxes over the KE region according to Bishop et al. (2017). Even if we first use the HadISST dataset, in this analysis we take advantage of the NOAA OISST product with a finer resolution that fits with the oceanic resolution of the model configurations here inspected.

Characteristics of the model used in this study: CMCC-CM2	
Configurations: HR: 'high resolution' VHR: 'very high resolution'	
	Atmosphere
Model	CAM4
Grid type	Grid point
Grid name	HR: 1° VHR: 0.25°
Nominal resolution (km)	HR: 100 VHR: 25
Resolution 50°N (km)	HR: 64 VHR:18
Vertical levels	26
Time step (min)	30
	Ocean-Sea ice
Ocean/Sea-ice model	NEMO3.6/CICE4.0
Grid type	Curvilinear
Numerical method	Finite difference
Grid name	ORCA025
Resolution	0.25°
Vertical levels	50
Time step (min)	20
Gent and McWilliams (1990) eddy parametrization	no
Horizontal momentum diffusion	-1.8×10^{11} m^4 s^{-1}
Background vertical eddy viscosity (m^2 s^{-1})	1.2×10^{-4}
Background vertical eddy diffusivity (m^2 s^{-1})	1.2×10^{-5}
Isopycnal tracer diffusivity (m^2 s^{-1})	300
Eddy-induced velocity coefficient (m^2 s^{-1})	n/a
Albedo of snow on sea-ice	No change
	Reference: Cherchi et al., 2018

TABLE 2. Model setups and simulations.

3.3 Results

3.3.1 Climatology

The Kuroshio Extension is known for shifting between a quasi-stationary state characterized by two very intense anticyclonic meanders east of Japan with a strong zonal penetration (elongated state), and a meandering state characterized by a reduced zonal penetration where the two anticyclonic meanders disappear (convoluted state). Using daily SSH fields, two indices are computed to characterize the KE state: the jet's latitudinal position (<φ>) and path length (LKE). These indices have been extensively used to highlight the KE bimodality (Qiu and Chen 2005; 2010; Pierini, 2006; 2014). Some degree of interdependency between these indices has been found. In particular, it has been observed that during the elongated state, a lower LKE is associated with a northward shifted jet, while during the convoluted state, the jet shifts southward and the LKE strongly increases due to the formation of eddies following the dissipation of the two anticyclonic meanders east of Japan in an inverse energy cascade process.

In the following, the two indices are computed in the upstream KE region (141-153°E) shown in Fig.18, where the highest jet variability is found due to the eddy-mean flow interaction. Downstream the jet is still highly varying, but it is more influenced by the broad-scale (i.e., non-eddy-related) variability. Weekly values of the LKE and <φ> indices have been diagnosed, using a reference SSH isoline to identify the jet's axis, corresponding to the maximum meridional SSH gradient in the upstream KE region (0.6 and 0.7 meters for HR and VHR respectively, while 0.9 meters in the observations). Simulated SSH climatology maps (Fig.18) show a latitudinal bias in the jet

positions, with both HR and VHR showing a southward displacement with respect to observations (~1 degree; see also the right panels of Fig.20). Despite the bias, we can assess that both models are able to qualitatively capture the mean SSH field in the Kuroshio and KE regions, with a strong anticyclonic meander South of Japan, a cyclonic circulation at the Kuroshio/Oyashio convergence forming the KE, and two anticyclonic gyres east of Japan. Although both are able to reproduce some of the jet's climatological features, there are some differences that deserve to be commented. The SSH is clearly underestimated in both the coupled models, more in HR than VHR; but HR better reproduces the mean field, with two, well distinguishable anticyclonic meanders east of Japan. In VHR the Upstream KE jet is more zonally elongated/less meandering, compared to HR and observations. If the SSH mean field provides information about the KE mean features, the EKE mean field computed from GSV data, provides a measure of the eddy-driven variability. In Fig.19 the simulated and observed EKE is computed as (Eq.2).

The magnitude and location of the observed EKE signature is well captured by HR and VHR, but both models display a substantial underestimation of its zonal extension. However, HR shows a slightly improved representation of the EKE pattern, in terms of its latitudinal extension, consistent with the more pronounced meandering character of the jet in HR, compared to VHR, the latter showing a more latitudinally confined and zonally stretched jet (Fig. 20). These preliminary results suggest that increasing the resolution of the atmospheric model does not translate into a clear improvement of the simulated KE mean state. In the next section the impact of resolution on the KE LFV is analyzed in detail.

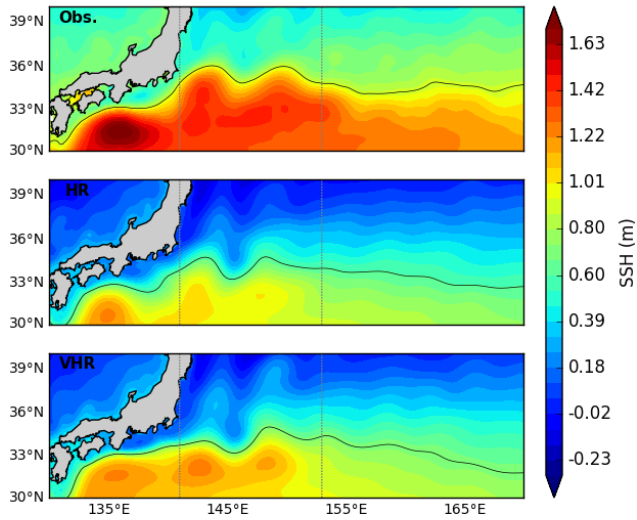

Fig.18. SSH maps averaged in time in the KE region for AVISO (top; 1993-2017), HR (middle; 0-100 yrs) and VHR (bottom; 0-100 yrs). Black line: KE jet reference isoline for each dataset (0.9; 0.6; 0.7 meters respectively). The vertical lines delimitate the upstream KE region (141-153°E).

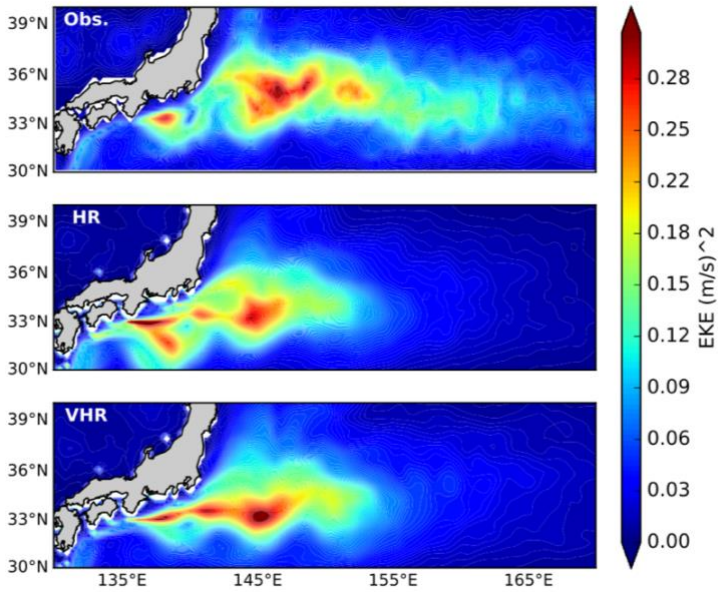

Fig.19. Geostrophic EKE maps averaged in time in the KE region for AVISO (top; 1993-2017), HR (middle; 0-100 yrs) and VHR (bottom; 0-100 yrs).

3.3.2 Frontal-scale variability of the jet

The frontal-scale variability of the jet is characterized through the aforementioned LKE and $<\varphi>$ indices. These are computed based on daily SSH and velocity fields, which are previously low-pass filtered with a boxcar averaging using a 7-day smoothing window, in order to filter out the daily variability. Figure 24 compares simulated and observed time series of the two indices. Note that model years bear no relation with the chronology shown

for the AVISO data, the latter covering the 1993-2017 period. In order to better emphasize the variability over interannual and longer timescales, yearly filtered time series (obtained via a 1-year moving window averaging) are also shown in Fig. 20.

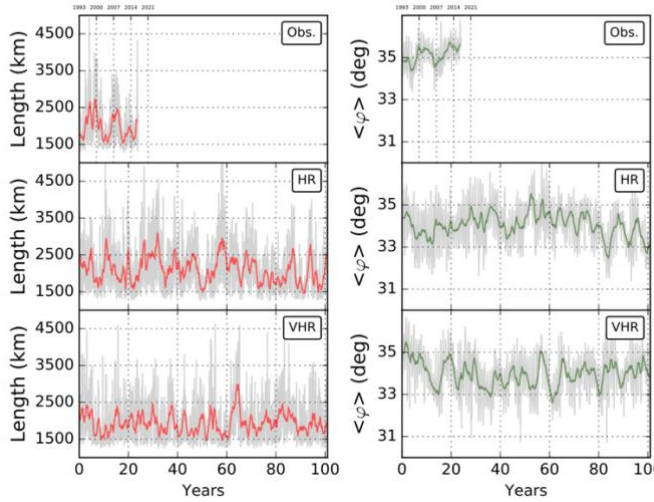

Fig.20. (Left) KE Path Length in AVISO (top), HR (center) and VHR (bottom). In grey weekly sampling, in red the 1-yr moving average after applying the boxcar filter. (Right) As before but for the KE mean latitudinal position. in green the 1-yr moving average after applying the boxcar filter.

A simple visual inspection of the LKE time series (Fig. 20) reveals that the simulated and observed indices share a fairly consistent kind of variability, with sharp weekly-scale fluctuations embedded within a lower frequency, multi-annual scale envelope, with the jet length varying between an approximately 1500 Km lower bound and higher values exceeding 3500 Km. Looking at the same signal in the frequency domain through an estimate

of the probability density function (PDF), the well-known KE bimodality (e.g. Qiu and Chen, 2005; 2010) emerges from the AVISO data set (Figs. 21, 22), characterized by a short, more frequent LKE regime, centered around a ~1500 Km length, and a longer (but less frequent) LKE regime, with a ~2200 Km length.

In order to allow a fair comparison between observations and models, accounting for the different lengths in the corresponding time series, we split the simulated LKE time series into 5 non-overlapping 20-year chunks and contrast the PDFs for each time segment and for observations. This comparison highlights the strong non-stationarity characterizing the modeled jet evolution, with different timeframes exhibiting substantial differences in their PDF distributions. The largest decadal changes are featured by HR, alternating epochs with bimodal (0-20 and 80-100 time frames in Fig.21) and trimodal (40-60 and 60-80 timeframes) LKE distributions. VHR, on the other hand, reveals a closer adherence to the observed jet bimodality across most of its temporal evolution. However, the typical LKE values characterizing the model regimes and their relative frequencies undergo considerable changes across the different time segments. This, in turn, determines a substantial blurring of the pluri-modal jet behavior when the whole 100-yr LKE time series is considered for both HR and VHR models, with the resulting PDFs showing a more Gaussian-like distribution (Fig. 21, left-most panel).

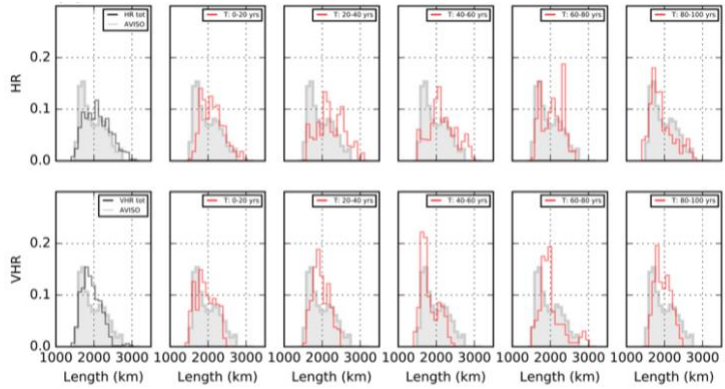

Fig.21. In red the Probability Density Function (PDF) for the KE Path Length in HR (top) and VHR (bottom) for 5 timeframes (0-20; 20-40; 40-60; 60-80; 80-100 yrs) evaluated against the AVISO PDF (filled grey, 1993-2017 yrs). Black line: PDF for the total timeseries (0-100 yrs) in HR (top) and VHR (bottom).

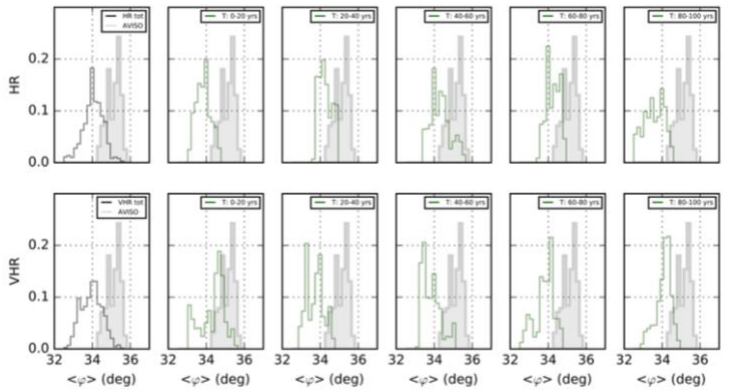

Fig.22. As Fig.21 but for the mean latitudinal position index.

Regarding the <φ> index (right panels in Fig.20 and Fig.22) both models show a clear (~1 degree) southward bias in the jet latitude. After splitting the 100-yr time series into 20-yr time segments, a pluri-modal behavior emerges in both models, including sporadic hints of bimodality (e.g., years 20-40 in HR and 60-80 in VHR, in Fig. 22). When considering the whole 100-yr time series, the overall distribution appears to be largely Gaussian for HR, while some hints of bimodality are found in VHR.

The highly not stationary nature of the jet is highlighted by the continuous wavelet transforms applied to these low-pass filtered indices (Fig.23), which provide a time-period representation for each continuous-time signal. This diagnostic evidences the way spectral features evolution over time, identifying time-varying patterns. The non-stationarity of the system is higher in VHR than HR in both the LKE and mean latitudinal position but in both the configurations the higher peaks of energy are attributed to processes which act on interannual-to-decadal time scales with peaks centered around 4-yrs and its multiples, that could be connected to a quasi-periodic external forcing.

Figs. 24 and 25 show the simulated weekly KE jet paths for a 20-year sample (corresponding to years 40-60, each panel corresponding to an individual model year) for HR and VHR, respectively. Bearing in mind the jet length properties, the sequence of yearly frames shows a consistent alternance between a convoluted (i.e., highly meandering, corresponding to high LKE values) and a zonally elongated (low LKE) states of the jet.

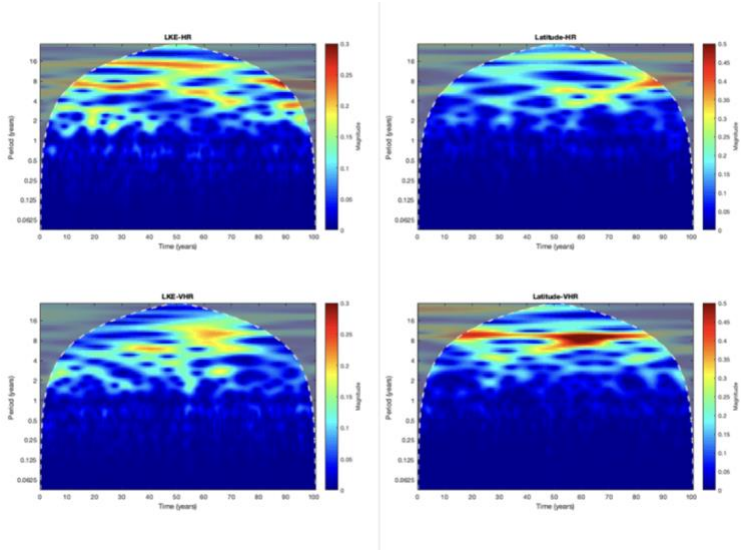

Fig.23. Continuous wavelet transforms applied to the low-pass filtered indices: LKE (left) and <φ> (right) for HR (top) and VHR (bottom).

Many studies (e.g. Qiu and Chen, 2010; Gentile et al., 2018) show that the LKE and <φ> indices are linked to each other; in the elongated state the jet is displaced northward and the LKE is lower, while in the convoluted state the jet shifts southward and the LKE increases. This led us to diagnose the Joint Probability Distribution (JPD) built upon the two analyzed jet indices, in order to identify the dominant regimes associated with the jet state using a bivariate <φ>-LKE phase space, for observations and models (Fig.26a-c). Consistent with the observed KE jet bimodality, the AVISO-based JPD features two well distinguishable peaks: a higher frequency one corresponding to a northward jet with lower LKE (identifying the elongated state), and a lower frequency one, shifted southward and with higher LKE, indicating a convoluted state (Fig. 26a). HR and VHR present more regimes

than AVISO, indicating the probability of the dynamical models to shift across multiple states (Fig.26b-c).

The JPDs associated with the two model simulations span different areas of the <φ>-LKE space. HR covers a range of LKE values that is reasonably consistent with the observational estimates, with two local maxima roughly corresponding to the ones in AVISO, but suffers from the previously discussed southward shift in the <φ> dimension. VHR, instead, under-represents the convoluted jet (high LKE) regime and further exacerbates (compared to HR) the southward displacement of the jet latitude. It is interesting to note that, despite the detected biases, both models maintain a certain degree of jet bimodality, consistent with the observational estimates. However, these results also suggest that increasing the horizontal resolution of the atmospheric model alone does not contribute to mitigate the biases deriving from the use of a standard resolution model. A major impact of resolution is to favor the occurrence of zonally elongated (low LKE) jet regimes, compared to the convoluted jet regime.

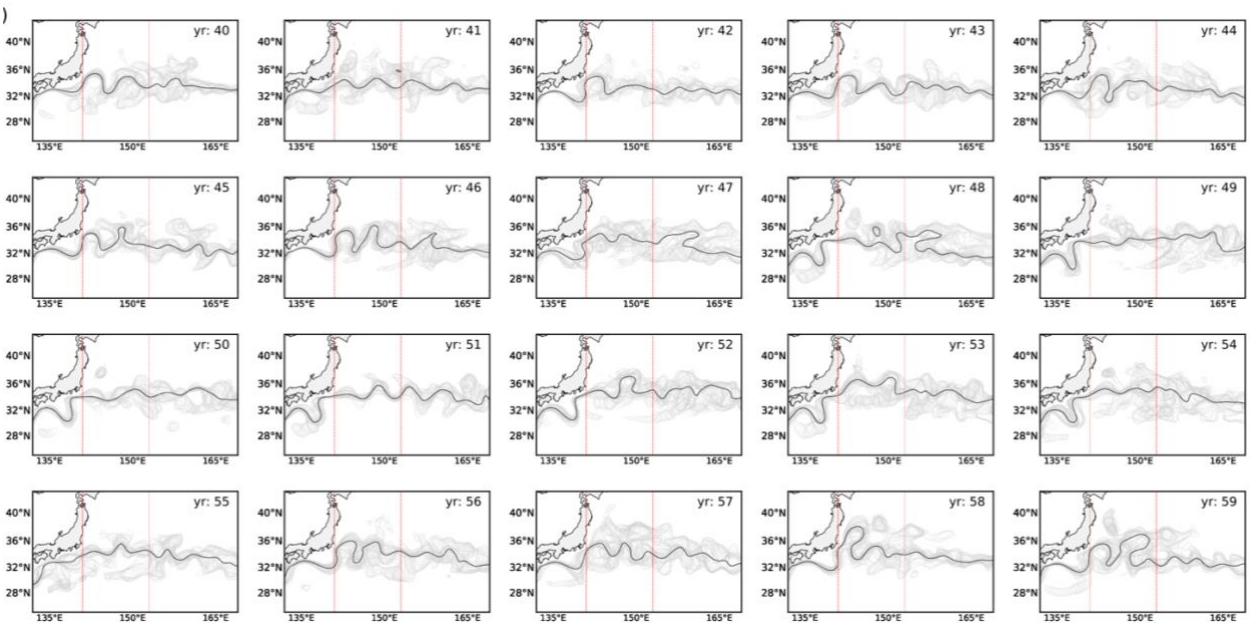

Fig.24. KE jet path for the 40-59 yrs timeseries in HR. Grey lines: weekly paths. Black line: mean path length for every year. The red lines delimit the upstream KE region.

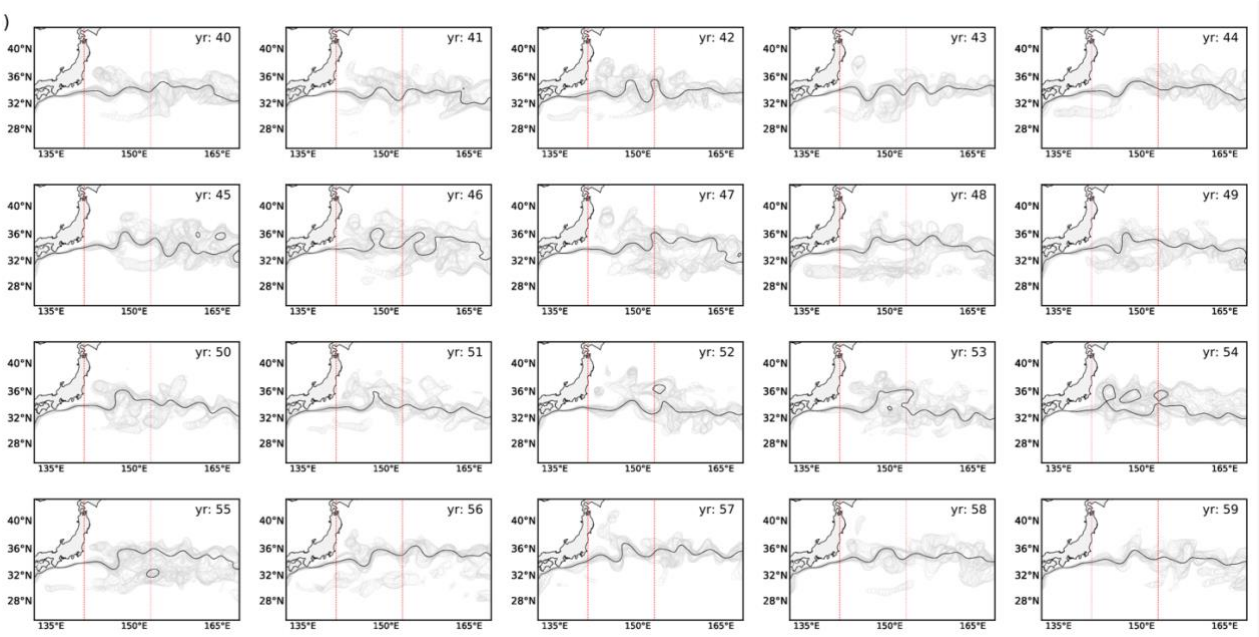

Fig.25. KE jet path for the 40-59 yrs timeseries in VHR. Grey lines: weekly paths. Black line: mean path length for every year. The red lines delimit the upstream KE region.

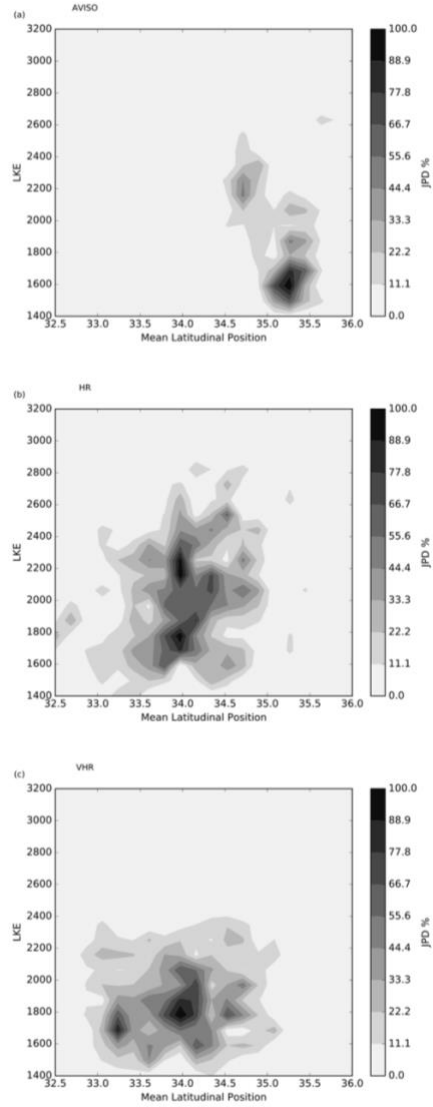

Fig.26. Joint Probability Distribution between the LKE and the mean latitudinal position in AVISO (a), HR (b) and VHR (c).

3.3.3 The influence of large-scale ocean-atmosphere variability on the jet

Several studies discuss the possible links between the frontal-scale variability of the jet and a variability mode of the extra-tropical North Pacific, the Pacific Decadal Oscillation (PDO), through a teleconnection mechanism provided by the propagation of baroclinic Rossby waves (e.g. Qiu, 2003; Qiu and Chen, 2005 and 2010; Ceballos et al. 2009 ; Andres et al., 2009; Wang et al., 2016). The PDO manifests itself with an SST anomaly pattern in the mid-latitude North Pacific, changing polarity with a typical decadal time scale. The PDO index is defined as the leading principal component of monthly mean SST anomalies in the North Pacific (north of 20°N).

The models' ability in reproducing the observed PDO pattern is assessed in Fig.27. Here, the PDO pattern is diagnosed through the leading EOF of SST anomalies in the [20N-70N] North Pacific domain, following Newman et al. (2016). Both simulated PDO patterns appear to be fairly consistent with observations. The only significant deviation is displayed by HR, featuring a spurious (negative) center of action off the eastern Japanese coast, which is absent in VHR.

The link between large-scale variability in the extra-tropical North Pacific, as represented by the PDO, and the KE jet (LKE index) is illustrated in Fig. 28, showing the coherence between the PDO phase, propagation of Rossby waves and KE jet length variability (LKE). Here, the PDO index, based on NOAA's extended reconstruction of SSTs (ERSST Version 4; Huang et al., 2014) is used (right panel) and is combined with SSH anomalies in the central Pacific (Hovmöller diagram; mid-panel) and the LKE index,

from AVISO, for the 1993-2017 period. This multi-panel plot is an updated version of Qiu and Chen (2010) and captures a well-established teleconnection between changes in the broad-scale PDO variability mode and the frontal-scale variability of the KE jet, via the westward propagation of baroclinic Rossby waves.

According to this picture, when the PDO is in a positive (negative) phase, SSH anomalies in the central part of the North Pacific are consistently lower (higher) than normal, and the KE path length increases (decreases), corresponding to a convoluted (elongated) state. These phases are found to be correlated with a meridional shift of the jet (Qiu, 2000), which is associated with changes in the gyre circulation structure: during the PDO+ (PDO-) phase, the Aleutian Low is stronger (weaker) than its normal, the Subtropical Gyre shifts southward (northward) and the negative (positive) SSH anomalies propagate westward, via baroclinic Rossby waves, ultimately affecting the KE variability (e.g. Qiu, 2000; Qiu and Chen; 2005; 2010; Di Lorenzo et al., 2007; Pierini, 2014). Through this mechanism, SSH anomalies generated by PDO fluctuations in the eastern-central Pacific (180-200°E) pace the decadal scale variability of the KE.

Based on this interpretative framework, next we assess whether the same mechanism holds for HR and VHR models as well. Fig. 29 shows the same diagnostics in Fig. 28, but for the two analyzed models. A number of similarities with the observational counterpart emerge, with evidence of PDO-correlated SSH features, travelling westward across the Pacific, getting amplified when reaching the neighborhood of the Japan coast. The final

impact on the LKE index is better illustrated in Fig. 30, showing two intervals where this chain of events is particularly well detected.

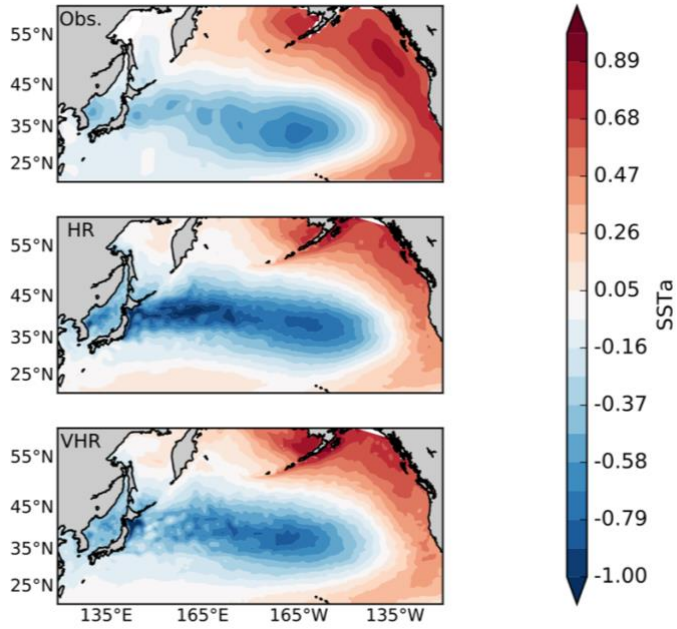

Fig.27. The first Empirical Orthogonal Function (EOF) for the SST anomalies field in the North Pacific Ocean in the observations (top), HR (center) and VHR (bottom).

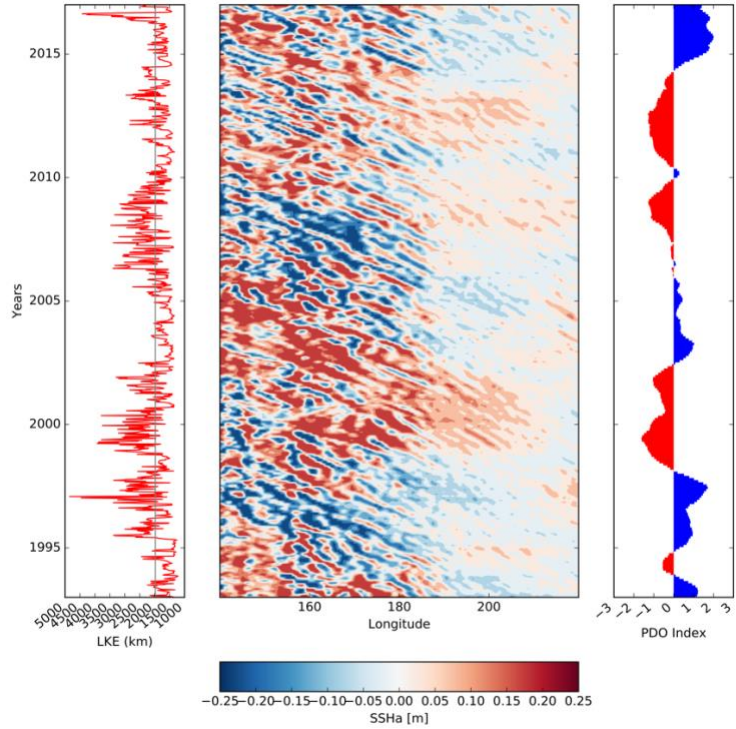

Fig.28. AVISO data. (Left) The LKE from 1993 to 2017 yrs (red line) and its mean value (in grey). (Center) The Hovmöller Diagram for the SSH anomalies in the upstream and downstream KE region [averaged between 32-34°N as Qiu and Chen, 2005]. (Right) The PDO Index computed as Newman et al., 2016.

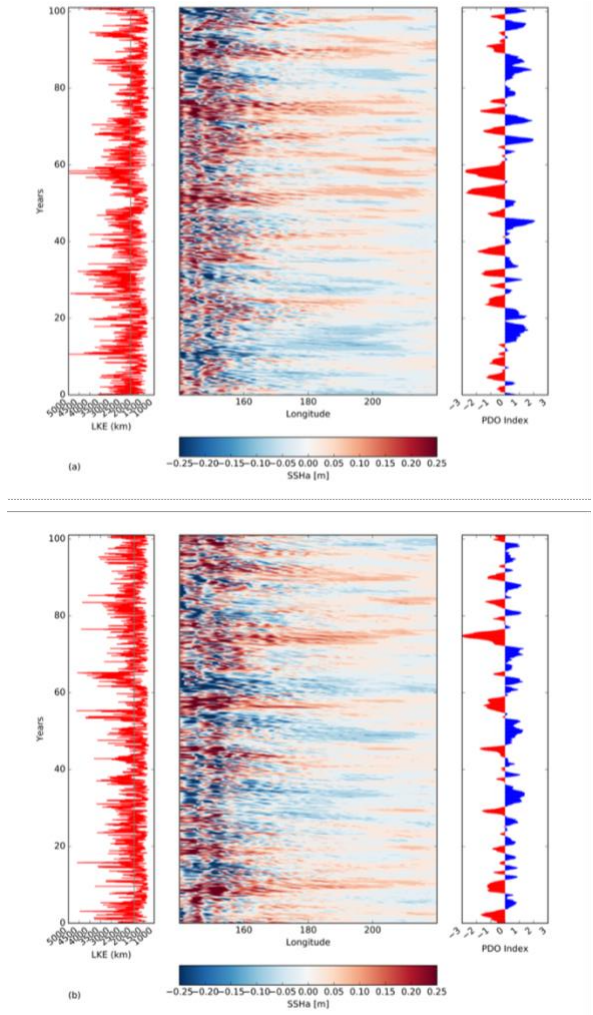

Fig.29. (a) HR data. (Left) The LKE computed in the 0-100 yrs timeseries (red line) and its mean value (in grey). (Center) The Hovmöller Diagram for the SSH anomalies in the upstream and downstream KE region [averaged between 32-34°N as Qiu and Chen, 2005]. (Right) The PDO Index computed as Newman et al., 2016. (b) As before but for the VHR dataset.

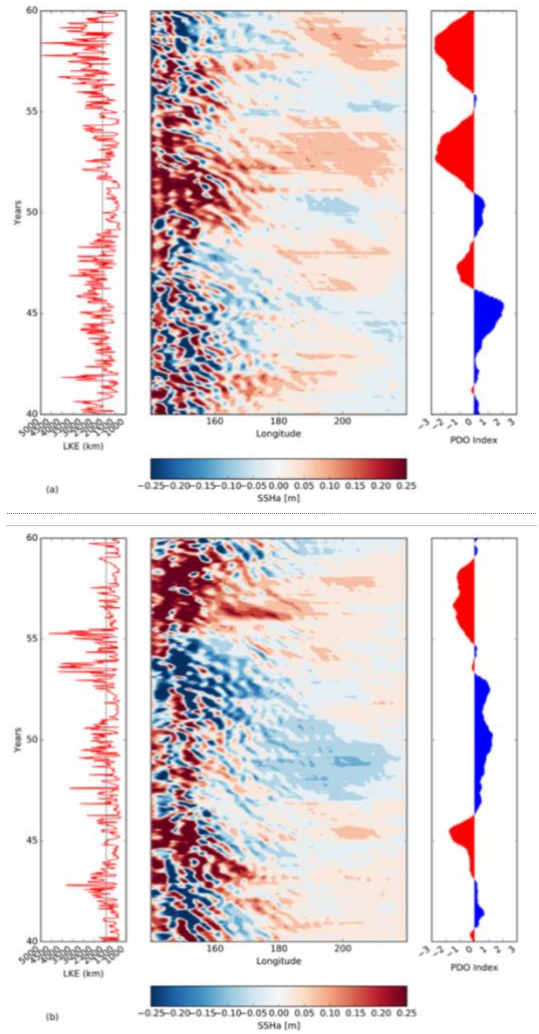

Fig.30. (a) HR data. As Fig. 33 but computed in the 40-60 yrs timeseries. (b) VHR data. As Fig. 33 but computed in the 40-60 yrs timeseries.

3.3.4 Ocean-Atmosphere interaction

The analysis presented in the previous sections is here complemented by looking at the air-sea interaction in a broad area surrounding the KE region. This aspect is relevant for both the frontal and broad-scale variability of the KE and can help interpreting the results presented in sections 3.3.2 and 3.3.3.

Here the work of Bishop et al. (2017) has been widely used as reference. The authors diagnose the lead-lag covariances between the SST and the SHF, and between SST tendency (SSTt) and Surface Heat Fluxes (SHF) in several key areas of the world ocean, encompassing the major WBC systems. These relationships reveal whether the ocean-atmosphere energy exchange is driven by the atmospheric synoptic-scale variability (weather) or by the oceanic internal variability. According to Bishop et al. (2017) findings, observations reveal that the atmosphere-driven regime dominates in the open ocean (e.g., subtropical gyre areas), in contrast with WBC regions which appear dominated by the ocean-driven regime.

Here we adopt the same approach to verify whether the expected SST (and SSTt)-SHF lead-lag relations are faithfully reproduced by the two HR and VHR models. Specifically related to our case study, the following questions are addressed: are HR and VHR able to capture the shift from the oceanic-regime to the atmospheric-regime moving from the KE region to the open ocean? What is the impact of the horizontal atmospheric resolution in the ocean-atmosphere interplay?

The monthly lead-lag correlations have been computed between the SST and SHF and the SSTt and SHF for both the coupled configurations and the

observations (see section 3.2.2 for details on the observational products used in this analysis). For the heat fluxes we use the positive upward convention. The lagged covariances are calculated as Bishop et al. (2017) and performed over the [120-180°E,20-60°N] domain, which includes both the upstream and downstream KE region.

The lagged covariance maps between the SST (SSTt) and the SHF (Figs. 31; 32) clearly show the ability of both the model configurations to reproduce the signatures of atmosphere-driven and ocean-driven regimes over the open ocean and the WBC regions, respectively, as expected (Bishop et al. (2017)) with some differences described below.

In the first part of this analysis the SST-SHF maps are discussed (Fig.31), these highlight the strengthening of the coupling in both the 100-yrs long configurations when evaluated against the observations (data from 1985 to 2013; as Bishop et al,2017); moreover, the covariances in VHR exceed the covariances in HR as expected, since processes on higher horizontal spatial scales are here resolved. The regions with the higher covariance are well picked by both the models but they are spread on wider areas meaning that HR and VHR overestimate the pattern of covariances. The dipole at +1-month lag (indicative of the shift between the two regimes) is well captured by either, with a consistent zonal extension of the oceanic-driven regime; instead the meridional extension is overestimated in VHR but not in HR (Fig.31). Those maps suggest that HR is more able than VHR to capture the distribution pattern of the SST-SHF lagged covariances, because the strengthening of the coupling introduces some biases; moreover, the analysis of the SSTt-SHF lead-lag covariance field (Fig.32) shows that HR is more

able to capture the SST tendency due to changes in the SHF in the KE region, suggesting that the lower is the resolution of the atmospheric model the better is the representation of the advection of SST, supporting the statement in section 3 that HR is more able to reproduce the KE frontal-scale variability. We argue that HR better captures the covariance relations due to an overly strong coupling strength in VHR, lead to an overestimation of the air-sea feedbacks (Fig.32). Next we focus on the open ocean (green dot; Figs.31; 32). Here the SST and the SHF are roughly in quadrature with each other around the 0 month lag and positive SHF (ocean cooling) is associated with negative SST tendency, identifying the atmospheric-driven regime; while moving to the WBC region (black diamond), the SHF acts damping the upper-ocean heat content anomalies generated by interior ocean processes, with the flux directly proportional to the SST itself, identifying the oceanic-driven regime (Bishop et al.,2017).

In agreement with Bishop et al. (2017), it is not surprising that HR and VHR are able to capture the two regimes because both resolve processes on scales less than 500 km.

Those results support the idea that enhancing resolution does not necessarily translate into an improved (more realistic) reproduction of physical processes. In the KE system we argue that this could be due to the nature of the KE variability: since in the WBC region the ocean-atmosphere interaction is mainly ocean-driven, by overestimating the air-sea feedbacks, VHR corrupts the degree of realism of the frontal variability of the jet. The PDO and the broad-scale variability instead are better captured by VHR due to the shift in the atmospheric-driven regime.

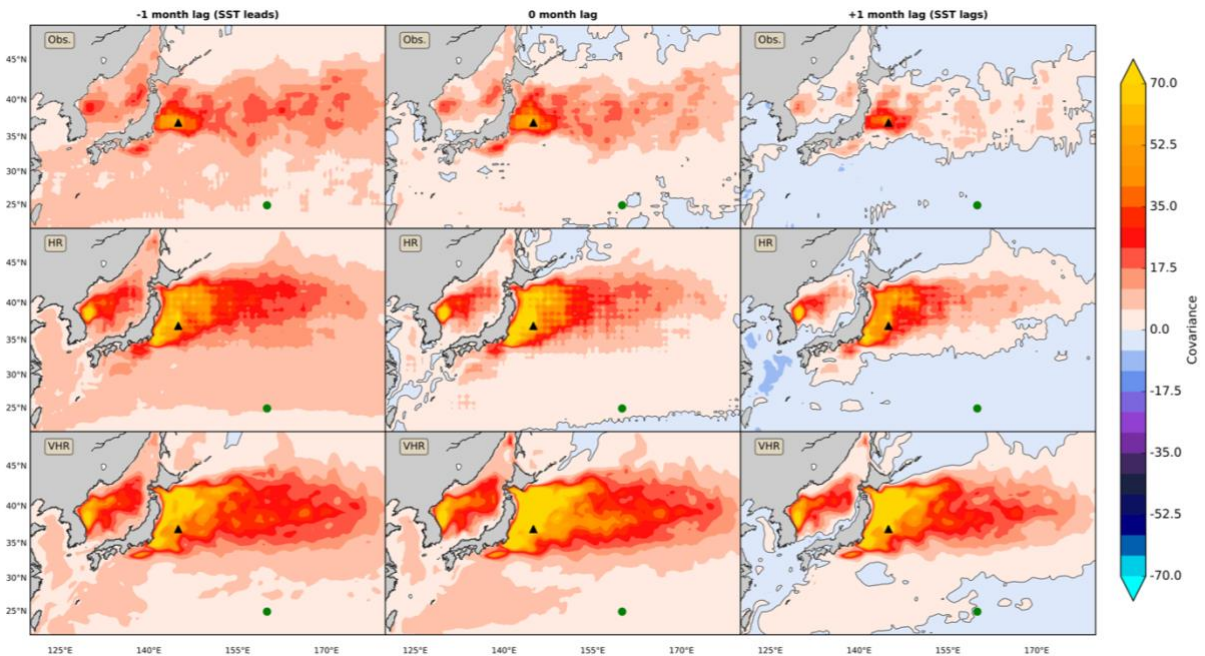

Fig.31. Lagged covariances (-1, 0, +1 lag from left to right) between the Sea Surface Temperature SST and the Surface Heat Fluxes SHF in the observations (top), HR (center) and VHR (bottom). Black triangle: WBC region; Green dot: Open Ocean Region.

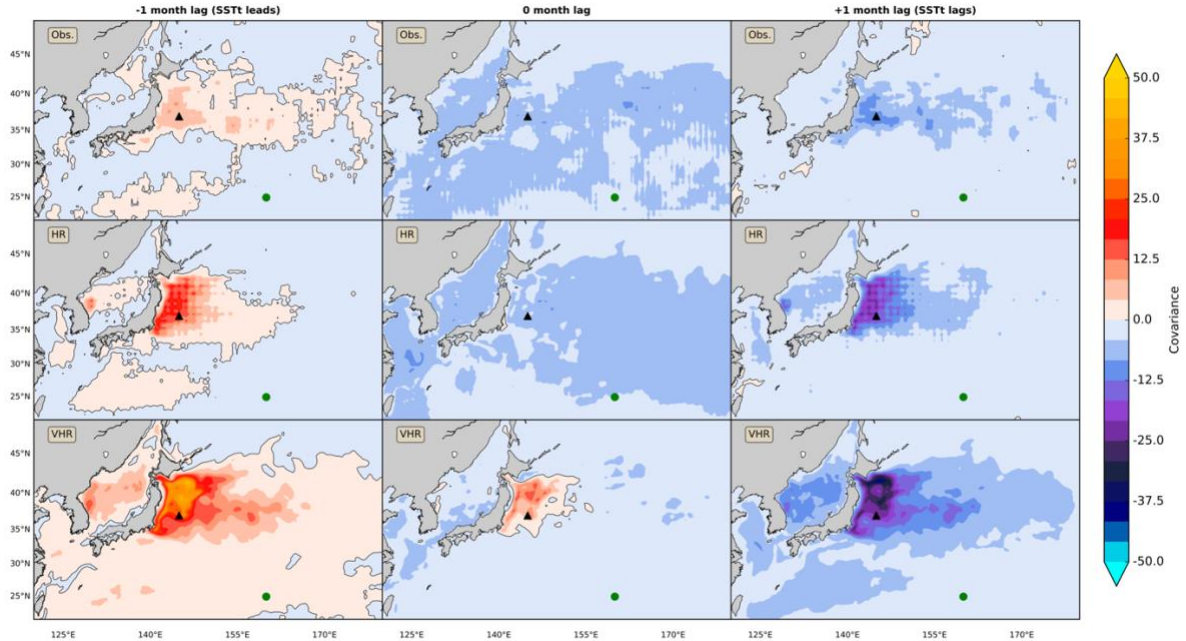

Fig.32. Lagged covariances (-1, 0, +1 lag from left to right) between the Sea Surface Temperature tendency SSTt and the Surface Heat Fluxes SHF in the observations (top), HR (center) and VHR (bottom). Black triangle: WBC region; Green dot: Open Ocean Region.-

3.4 Discussion and conclusions

The main goal of this chapter was the investigation of the KE in the context of a fully coupled system, as represented by a state of the art CGCM. In this context, the impact of the horizontal resolution of the atmospheric model on the KE system has been assessed.

Several studies (e.g. Delworth et al., 2012; Small et al., 2014; Haarmsa et al., 2016) have shown that increasing the resolution introduce many benefits in the simulation of several phenomena. In contrast, other works show that increasing the resolution has many benefits, but this does not happen unanimously on all processes (e.g. Ma et al., 2016; Vannière et al., 2018).

In this study, we suggest that when increasing the resolution of the atmospheric component, opposite impacts can emerge in the simulation of different phenomena. We show that coupling the same oceanic model with two atmospheric models at different resolution does not imply that the higher is the resolution, the better is the simulation; but on the contrary, many features of the dynamical system can be better resolved at lower resolutions.

The main findings of this work are here summarized:

- The KE's climatology is well captured by both the configurations but enhancing the resolution the jet is less meandering/zonally elongated.
- The frontal-scale variability in HR and VHR is consistent with the observational estimates but enhancing the resolution the elongated state is favored compared to the convoluted state.

- A pluri-modal behavior emerges in both models, including sporadic hints of bimodality. HR covers a range of LKE values consistent with the observational estimates but suffers from a bias in the latitudinal position of the jet. VHR, instead, under-represents the convoluted jet regime and further exacerbates (compared to HR) the southward shift of the jet's position. Despite these biases, HR and VHR maintain a certain degree of jet bimodality, consistent with the observations.

- The PDO acts as pacemaker of the KE LFV, in agreement with previous studies (e.g. Qiu and Chen; 2005; 2010; Pierini, 2014). Increasing the resolution of the atmospheric component the PDO is more realistic. The teleconnection mechanism provided by the Rossby waves propagation is quite well captured by both the models.

- The air-sea interaction is more realistic in HR, since the stronger coupling implied in VHR overestimates the ocean-atmosphere feedbacks.

Therefore, this study supports the idea that increasing the resolution is not always beneficial. In fact, many features of the KE are better captured by the coarser model. We support that in the analyzed region the atmosphere does not lead the oceanic variability at every timescale and spatial scale, justifying different sensitivities for different processes. In fact, this study in agreement with Bishop et al. (2017) highlights that in the KE region the variability is mainly oceanic-driven, while in the open ocean the atmosphere leads changes in the coupled system. The atmospheric resolution plays a marginal role in the KE LFV compared to the oceanic resolution, which in contrast introduces many benefits in the degree of realism of the KE LFV

as shown by previous studies (e.g. Haarmsa et al., 2016) but not discussed in this work.

In this context, future studies could be devoted to better understand the processes behind the 'selectivity' of the model resolution in improving or decreasing the degree of realism of the KE LFV.

Chapter 4

4.1 Discussion and conclusions

This thesis is focused on the Kuroshio Extension system, one of the regions of the world ocean with the highest eddy kinetic energy level. Its large-scale interannual changes are able to enhance the midlatitude coupled ocean-atmosphere system (Xie et al. 2000), playing therefore a key role in the climate variability.

Being the KE a WBCs system, the ocean variability leads the total variability of the coupled ocean-atmosphere system in the KE region (Bishop et al., 2017). Therefore, it is really important to understand the mechanisms behind the KE LFV in order to predict changes in the atmosphere at mid-latitudes. At the same time, the KE LFV is found to be lag-correlated with the PDO pattern of variability (Qiu and Chen, 2010), opening a debate regarding the role played by intrinsic oceanic mechanisms and external atmospheric forcings in the total variability of the jet.

Inspecting first the interplay between the ocean and the atmosphere in the KE LFV from the dynamic systems theory point of view, and finally examining in detail the role of the atmosphere in the total variability of the system, in this thesis we show in agreement with previous studies (e.g. Pierini, 2014; Bishop, 2017) that the KE LFV is an intrinsic oceanic mechanism paced by external atmospheric forcings and that changes in the horizontal resolution of the atmospheric model have not a relevant impact in the KE's degree of realism, suggesting that the atmosphere plays a marginal role in the

variability of the jet and that the increased atmospheric resolution by itself does not reflect into an improved air-sea interaction in this region.

The first part of this thesis aims to answer the scientific question:

What is the relative role of the internal oceanic mechanisms and external atmospheric forcing in driving the KE variability?

Inspecting the KE LFV in the OCCIPUT dataset (section 2.2.1), it appears that the system oscillates between the elongated and the convoluted states mainly driven by intrinsic oceanic mechanisms. Analyzing in detail the KE autonomous and nonautonomous systems, two main equilibrium points are populated by the jet in both the configurations. The KE jet shifts slowly between two quasi-stationary states forced by a climatological atmospheric forcing; while introducing its contribution, the KE jet explores the phase space following many orbits with a low persistence and without a prior direction. Moreover, the atmosphere acts tilting and reducing the region of the phase space explored by the KE LFV. In fact, comparing the location of the two modes in both the configurations, it is evident that in the nonautonomous case provided by OCCITENS the two modes are rotated in a phase space that is smaller compared to the phase space explored in OCCICLIM.

The jet bimodality appears to be an intrinsic feature of the oceanic variability, but the atmosphere paces this variability shaping the phase space explored by the attractor through local air-sea interactions and Rossby wave train propagation.

The eddy-mean flow interaction plays a fundamental role in the KE LFV, therefore a good strategy to adopt in future studies could be to increase the oceanic resolution of the ensemble simulations moving from an eddy-permitting (OCCIPUT like) to an eddy-resolving system. This amelioration could likely affect the degree of realism of the KE and the predictability of the system. Other improvements can also be introduced having a larger number of ensemble members. The higher is the number of members, the better is the ability to study the KE system from the dynamical systems' point of view.

In the second part of this work we address the following question:

What is the impact of the coupling of an ocean model with an atmospheric model with different horizontal resolutions on the KE dynamical system?

To achieve this goal two coupled model configurations have been analyzed in the PRIMAVERA project framework (section 3.2.1).

Several studies show the beneficial effects introduced by a higher resolution both in the atmospheric and oceanic components in the KE region, suggesting that increasing the resolution, the models capture better the dynamics in this area. In contrast, we demonstrate in chapter 3 that this behavior of the models is not uniformly applicable to every resolution and phenomenon. In fact, investigating the KE region in two coupled model configurations with same resolution of the oceanic component and a different horizontal resolution in the atmosphere, we assess that increasing the resolution not every phenomenon has benefits. In addition, some KE's features are better captured by the coarser model (e.g. VHR dumps the

convoluted jet regime and compared to HR exacerbates the southward shift of the jet's position).

Possible links between the KE and external atmospheric forcings have been investigated, showing that the PDO in both the configurations acts as pacemaker of the KE LFV, in agreement with previous studies (e.g. Qiu and Chen; 2005; 2010; Pierini, 2014). The teleconnection mechanism provided by the Rossby waves propagation is quite well captured by both the models.

We found that the atmospheric resolution plays a marginal role in the KE dynamical system when compared with the oceanic resolution, whose role in contrast is crucial for the degree of realism of the KE LFV.

This is in agreement with the previous results (Chapter 2) that interpret the KE LFV as an intrinsic mechanism paced by the atmosphere. We suppose that a coupled model with a coarser atmospheric resolution reproduces better some features of the KE LFV because its variability is led by internal oceanic mechanisms and the oceanic resolution used in both the configurations is able to capture the intrinsic variability of the ocean in this region.

With this study we have made some progress in the state-of-the-art and the current scientific knowledge, understanding both the nature of the KE LFV and the impacts of the atmospheric horizontal resolution on the KE system, which is important to identify the needs of the next generation models to capture and predict the KE LFV.

Future works can be devoted to finding a good strategy to predict the KE LFV and investigate its sensitivity under climate change scenarios. They would significantly contribute to dealing with problems that actually the

climate community, the governments and people have to face every day. Impacts of the KE changes due to the climate change on climate extremes, such as heat waves, droughts, floods and cyclones, would reveal the vulnerability and exposure of some ecosystems and many human systems to current climate variability.

References

Andres M, Park J H, Wimbush M, Zhu X H, Nakamura H, Kim K, Chang K I., 2009: Manifestation of the Pacific decadal oscillation in the Kuroshio. Geophys Res Lett, 36: L16602

Barnier, B., Siefridt, L., and Marchesiello, P., 1995: Thermal forcing for a global ocean circulation model using a three-year climatology of ECMWF analyses, J. Mar. Syst., 6, 363–380, doi:10.1016/0924- 7963(94)00034-9.

——, Madec, G., Penduff, T., Molines, J.-M., Treguier, A.- M., Le Sommer, J., Beckmann, A., Biastoch, A., Böning, C., Dengg, J., Derval, C., Durand, E., Gulev, S., Remy, E., Talandier, C., Theetten, S., Maltrud, M., McClean, J., and De Cuevas, B., 2006: Impact of partial steps and momentum advection schemes in a global ocean circulation model at eddy permitting resolution, Ocean Dynam., 56, 543–567.

Batchelor, G. K., 1967: An Introduction to Fluid Dynamics, Cambridge University Press, 615 + xvii pp.

Berloff, P.S., 2005: Random-forcing model of the mesoscale oceanic eddies. Journal of Fluid Mechanics, 529, pp.71-95. 881 Berloff, P. S., A. M. Hogg, and W. Dewar, 2007: The turbulent oscillator: A 882 mechanism of low-frequency variability of the wind-driven ocean gyres. J. 883 Phys. Oceanogr., 37, 23632386.

Bessières, L., Leroux, S., Brankart, J.-M., Molines, J.-M., Moine, M.-P., Bouttier, P.-A., Penduff, T., Terray, L., Barnier, B., and Sérazin, G., 2017: Development of a probabilistic ocean modelling system based on NEMO 3.5: application at eddying resolution, Geosci. Model Dev., 10, 1091–1106, https://doi.org/10.5194/gmd-10-1091-2017.

Bishop, S. P., R. J. Small, F. O. Bryan, and R. A. Tomas, 2017: Scale dependence of midlatitude air–sea interaction. J. Climate, 30, 8207–8221, https://doi.org/10.1175/JCLI-D-17-0159.1

Brankart, J.-M., Candille, G., Garnier, F., Calone, C., Melet, A., Bouttier, P.-A., Brasseur, P., and Verron, J., 2015: A generic approach to explicit

simulation of uncertainty in the NEMO ocean model, Geosci. Model Dev., 8, 1285–1297, doi:10.5194/gmd-8-1285- 2015.

Burkey, J., 2013: LOWESS, locally weighted scatterplot smoothing for linear and non- linear data (enhanced). http://www.mathworks.com/matlabcentral/ fileexchange/22470 (accessed February 2013).

Ceballos, L. I., E. Di Lorenzo, C. D. Hoyos, N. Schneider, and B. Taguchi, 2009: North Pacific Gyre Oscillation synchronizes climate fluctuations in the eastern and western boundary systems. J. Climate, 22, 5163–5174.

Cessi, P., G. R. lerley and W. R. Young., 1987: A model of the inertial recirculation driven by potential vorticity anomalies. J. Phys. Oceanogr., 17, 1640-1652.

——, R. V. Condie and W. Young, 1990: Dissipative dynamics of western boundary currents. J. Mar. Res., 48, 677– 700.

Chao, S.-Y., 1984: Bimodality of the Kuroshio. J. Phys. Oceanogr., 14, 92–103, https://doi.org/10.1175/1520-0485(1984)014,0092: BOTK.2.0.CO;2.

Chau-Ron Wu, 2013: Interannual modulation of the Pacific Decadal Oscillation (PDO) on the low-latitude western North Pacific, Progress in Oceanography, Volume 110, 2013, Pages 49-58, ISSN 0079-6611, https://doi.org/10.1016/j.pocean.2012.12.001.

Cherchi A, Fogli PG, Lovato T, Peano D, Iovino D, Gualdi S, Masina S, Scoccimarro E, Materia S, Bellucci A, Navarra A, 2018: Global mean climate and main patterns of variability in the CMCC- CM2 coupled model. J Adv Model Earth Syst 11:185. https://doi. org/10.1029/2018MS001369

CMCC, 2018a: CMCC-CM2-HR4 model output prepared for CMIP6 HighResMIP hist-1950. Earth System Grid Federation. http:// cera-www.dkrz.de/WDCC/meta/CMIP6/CMIP6.HighResMIP. CMCC.CMCC-CM2-HR4.hist-1950

——, 2018b: CMCC CMCC-CM2-VHR4 model output prepared for CMIP6 HighResMIP hist-1950. Earth System Grid Federation. http://cera-www.dkrz.de/WDCC/meta/CMIP6/CMIP6.HighResMIP.CMCC.CMCC-CM2-VHR4.hist-1950

Delworth, T. L., Rosati, A., Anderson, W., Adcroft, A. J., Balaji, V., Benson, R., Dixon, K., Griffies, S. M., Lee, H.-C., Pacanowski, R. C., Vecchi, G. A., Wittenberg, A. T., Zeng, F., and Zhang, R., 2012: Simulated climate and climate change in the GFDL CM2.5 high- resolution coupled climate model, J. Climate, 25, 2755–2781, doi:10.1175/JCLI-D-11-00316.1.

Deser, C. and M. L. Blackmon, 1995: On the relationship between tropical and North Pacific sea surface variations. J. Climate, 8, 1677–1680.

——, M. A. Alexander and M. S. Timlin, 1996: Upper-ocean thermal variations in the North Pacific during 1970– 1991. J. Climate, 8, 1840–1855.

——, M. A. Alexander, and M. S. Timlin, 1999: Evidence for a wind-driven intensification of the Kuroshio Current Extension from the 1970s to the 1980s. J. Climate, 12, 1697–1706.

Dewar, W.K., 2003: Nonlinear mid-latitude ocean adjustment, J. Phys. 911 Oceanogr., 33, 1057-1082.

——, 2005: Mechanisms of decadal variability of the wind-driven ocean circulation. J. Phys. Oceanogr., 35, 512–531

Di Lorenzo E., Schneider N., Cobb K. M., Chhak, K, Franks P. J. S., Miller A. J., McWilliams J. C., Bograd S. J., Arango H., Curchister E., Powell T. M. and P. Rivere, 2008: North Pacific Gyre Oscillation links ocean climate and ecosystem change. Geophys. Res. Lett., 35, L08607, doi:10.1029/2007GL032838.

Dijkstra A.H., Ghil M, 2005a: Low-frequency variability of the large-scale ocean circulation: A dynamical systems approach. Rev. Geophys., 43, RG3002.

——, 2005b: Nonlinear Physical Oceanography. Springer, 532 pp.

——, Ghil M, 2005: Low-frequency variability of the large-scale ocean circulation: A dynamical systems approach. Rev. Geophys., 43, RG3002.

Drótos, G., Bódai, T., Tél, T., 2016: Quantifying nonergodicity in nonautonomous dissipative dynamical systems: An application to climate change, Phys. Rev. E 94, 022214.

Dussin, R., Barnier, B., Brodeau, L., and Molines, J.-M., 2016: The making of Drakkar forcing set DFS5, DRAKKAR/MyOcean Report, 01-04-16, LGGE, Grenoble, France.

Eyring, V., Bony, S., Meehl, G. A., Senior, C. A., Stevens, B., Stouffer, R. J., and Taylor, K. E., 2016: Overview of the Coupled Model Intercomparison Project Phase 6 (CMIP6) experimental design and organization, Geosci. Model Dev., 9, 1937–1958, https://doi.org/10.5194/gmd-9-1937-2016.

Frankignoul, C., and N. Sennéchael, 2007: Observed influence of North Pacific SST anomalies on the atmospheric circulation. J. Climate, 20, 592-606.

Fu, L.-L., and D. B. Chelton, 2001: Large-scale ocean circulation. Satellite Altimetry and Earth Science, L.-L. Fu and A. Cazenava, Eds., Academic Press, 133–169.

Gentile, V., S. Pierini, P. de Ruggiero, and L. Pietranera, 2018: Ocean modelling and altimeter data reveal the possible occurrence of intrinsic low-frequency variability of the Kuroshio Extension. Ocean Modell., 131, 24–39, https://doi.org/10.1016/ j.ocemod.2018.08.006.

Ghil, M., 2019: A century of nonlinearity in the geosciences. Earth and Space Science. 6. https://doi.org/10.1029/2019EA000599

Grégorio, S., Penduff, T., Sérazin, G., Molines, J. M., Barnier, B., and Hirshi, J., 2015: Intrinsic variability of the Atlantic meridional overturning circulation at interannual-to- mul- tidecadal timescales, J. Phys. Oceanogr., 45, 1929–1946, doi:10.1175/JPO-D-14-0163.1.

Haarsma, R. J., Roberts, M. J., Vidale, P. L., Senior, C. A., Bellucci, A., Bao, Q., Chang, P., Corti, S., Fučkar, N. S., Guemas, V., von Hardenberg, J., Hazeleger, W., Kodama, C., Koenigk, T., Leung, L. R., Lu, J., Luo, J.-J., Mao, J., Mizielinski, M. S., Mizuta, R., Nobre, P., Satoh, M., Scoccimarro, E., Semmler, T., Small, J., and von Storch, J.-S.: High Resolution Model

Intercomparison Project (HighResMIP v1.0) for CMIP6, Geosci. Model Dev., 9, 4185–4208, https://doi.org/10.5194/gmd-9-4185-2016, 2016.

Hilborn R.C., 2000: Chaos and Nonlinear Dynamics. An Introduction for Scientists and Engineers. Department of Physics Amherst College. Oxford University Press.

Hogg, A. M., P. D. Killworth, J. R. Blundell, and W. K. Dewar, 2005: Mechanisms of decadal variability of the wind-driven ocean circulation. J. Phys. Oceanogr., 35, 512–531.

Hunke E, Lipscomb W, Turner A, Jeery N, Elliott S, 2015: CICE: the Los Alamos sea ice model, documentation and software users manual, Version 5.1. (Tech. Rep. LA-CC-06-012.). Tech. rep., Los Alamos National Laboratory

Hurlburt, H. E., A. J. Wallcraft, W. J. Schmitz, P. J. Hogan and E. J. Metzger, 1996: Dynamics of the Kuroshio/Oyashio current system using eddy-resolving models of the North Pacific Ocean. J. Geophys. Res., 101, 941–976.

Jiang, S., F. F. Jin and M. Ghil, 1995: Multiple equilibria, periodic, and aperiodic solutions in a wind-driven, double- gyre, shallow-water model. J. Phys. Oceanogr., 25, 764– 786.

Kawai, H., 1972: Hydrography of the Kuroshio Extension. p. 235–354. In Kuroshio—Its Physical Aspects, ed. by H. Stommel and K. Yoshida, University of Tokyo Press.

Latif, M., and T. P. Barnett, 1994: Causes of decadal climate variability over the North Pacific and North America. Science, 266, 634–637.

——, and T. P. Barnett, 1996: Decadal climate variability over the North Pacific and North America: Dynamics and predictability. J. Climate, 9, 2407–2423.

Leroux, S., T. Penduff, L. Bessieres, J. Molines, J. Brankart, G. Serazin, B. Barnier, and L. Terray, 2018: Intrinsic and Atmospherically Forced Variability of the AMOC: Insights from a Large-Ensemble Ocean Hindcast. J. Climate, 31, 11831203.

Levitus, S., 1982: Climatological Atlas of the World Ocean. NOAA Prof. Paper No. 13, U.S. Government Printing Of- fice, Washington, D.C., 173 pp.

Lorenz, E. N., 1963: Deterministic nonperiodic flow, J. Atmos. Sci., 20, 130–141.

——,1969a: Atmospheric predictability as revealed by naturally occurring analogues, J. Atmos. Sci., 26, 636–646, 1969.

——, 1969b: The predictability of a flow which possesses many scales of motion. Tellus, 21,289-307., 1982: Atmospheric predictability experiments with a large numerical model. Tellus, 34, 505-513.

Lorenz, E. N., 1963: Deterministic nonperiodic flow. J. Atmos. Sci. 20, 130–141.

——, 1969: Atmospheric predictability as revealed by naturally occurring analogues. Journal of the Atmospheric sciences, 26(4), 636-646.

——, 1991: Dimension of weather and climate attractors, Nature, 353, 241, https://doi.org/10.1038/353241a0.

Liebovitch, L. S. & Toth, T., 1989: A fast algorithm to determine fractal dimensions by box counting. Phys. Lett. A 141, 386–390.

Ma, J., and H. Xu. 2012. "The Relationship between Meridional Displacement of the Oceanic Front in Kuroshio Extension during Spring and Atmospheric Circulation in East Asia." Journal of the Meteorological Sciences 32: 375–384.

——, Xu H., Dong C et al. ,2015: Atmospheric responses to oceanic eddies in the Kuroshio extension region. J Geophys Res 120:6313–6330

——, Xu H., Dong C., 2016a: Seasonal variations in atmospheric responses to oceanic eddies in the Kuroshio extension. Tellus A 68:31563

——, Jing, Z., Chang, P., Liu, X., Montuoro, R., Small, R. J., Bryan, F. O., Greatbatch, R. J., Brandt, P., Wu, D., Lin, X., and Wu, L., 2016b: Western boundary currents regulated by interaction between ocean eddies and the atmosphere, Nature, in press.

Mantua, N J, Hare, S R, Zhang, Y, Wallace, J M, and Francis, R C, 1997: A Pacific Interdecadal Climate Oscillation with Impacts on Salmon, Bull. Am. Meteorol. Soc., 78, 1069 – 1079.

——, & Hare, S.R. Journal of Oceanography, 2002: The Pacific Decadal Oscillation, 58: 35. https://doi.org/10.1023/A:1015820616384

Masuda, A., 1982: An interpretation of the bimodal character of the stable Kuroshio path. Deep Sea Res., 29A, 471–484, https://doi.org/10.1016/0198-0149(82)90071-1.

Mass, C. F., D. Ovens, K. Westrick, and B. A. Colle, 2002: Does increasing horizontal resolution produce more skillful forecasts: The results of two years of real-time numerical weather prediction over the Pacific Northwest. Bull. Amer. Meteor. Soc., 83, 407–430, https://doi.org/10.1175/1520-0477(2002)083<0407:DIHRPM>2.3.CO;2.

Miller, A. J., D. R. Cayan, T. P. Barnett, N. E. Graham and J. M. Oberhuber, 1994: Interdecadal variability of the Pacific Ocean: model response to observed heat flux and wind stress anomalies. Climate Dyn., 9, 287–302.

——, D. R. Cayan, and W. B. White, 1998: A westward- intensified decadal change in the North Pacific thermocline and gyre-scale circulation. J. Climate, 11, 3112–3127.

——, D. R. Cayan and W. B. White, 1998: A westward-intensified decadal change in the North Pacific thermocline and gyre-scale circulation. J. Climate, 11, 3112– 3127.

Milnor, J., 1985: On the concept of attractor, Commun. Math. Phys., 99, 177–195.

Nakamura, H., T. Sampe, Y. Tanimoto, and A. Shimpo. 2004: "Observed Associations among Storm Tracks, Jet Streams and Midlatitude Oceanic Fronts." In Earth's Climate: The Ocean– Atmosphere Interaction, edited by C. Wang, S.-P. Xie, and J. A. Carton, 329–345. Geophys Monogr 147. Washington, DC: AGU.

Nathan J. and Steven R. H., 2002: "The Pacific Decadal Oscillation." Journal of Oceanography 58: 35-44.

Neale RB, 1049 Richter J, Park S, Lauritzen PH, Vavrus SJ, Rasch PJ, Zhang M, 2013: The mean climate of the Community Atmosphere Model (CAM4) in forced SST and fully coupled experiments. Journal of Climate 26:5150{5168, DOI 10.1029/2007GL031138.

Newman, M., M.A. Alexander, T.R. Ault, K.M. Cobb, C. Deser, E. Di Lorenzo, N.J. Mantua, A.J. Miller, S. Minobe, H. Nakamura, N. Schneider, D.J. Vimont, A.S. Phillips, J.D. Scott, and C.A. Smith, 2016: The Pacific Decadal Oscillation, Revisited. J. Climate, 29, 4399–4427, https://doi.org/10.1175/JCLI-D-15-0508.1

Nonaka, M., H. Nakamura, Y. Tanimoto, T. Kagimoto, and H. Sasaki, 2006: Decadal variability in the Kuroshio–Oyashio Extension simulated in an eddy-resolving OGCM. J. Climate, 19, 1970–1989.

——, H. Sasaki, B. Taguchi, and H. Nakamura, 2012: Potential predictability of interannual variability in the Kuroshio Extension jet speed in an eddy-resolving OGCM. J. Climate, 25, 3645–3652.

O'Reilly, C. H. and Czaja, A., 2015: The response of the Pacific storm track and atmospheric circulation to Kuroshio Extension variability. Q.J.R. Meteorol. Soc., 141: 52-66. doi:10.1002/qj.2334.

Oleson KW, Lawrence DM, Bonan GB, Drewniak B, Huang M, Koven C, et al., 2013: Technical description of version 4.5 of the Community Land Model (CLM). Tech. rep., NCAR Technical Note.

Pedlosky, J. P. 1987: Geophysical Fluid Dynamics, 2nd ed. Springer Verlag, 710 + xiv pp.

Penduff, T., Juza, M., Barnier, B., Zika, J., Dewar, W. K., Treguier, A.-M., Molines, J.-M., and Audiffren, N., 2011: Sea level expression of intrinsic and forced ocean variabilities at interannual time scales, J. Climate, 24, 5652–5670.

——, Barnier, B., Terray, L., Bessie`res, L., Se´razin, G., Gre- gorio, S., Brankart, J., Moine, M., Molines, J., and Brasseur, P., 2014: Ensembles of

eddying ocean simulations for climate, CLIVAR Exchanges, Special Issue on High Resolution Ocean Climate Modelling, 19.

——, G. Serazin, S. Leroux, S. Close, J.-M. Molines, B. Barnier, L. Bessieres, L. Terray, and G. Maze, 2018: Chaotic variability of ocean heat content: climate-relevant features and observational implications. Oceanography, 31(2).

Pierini S., 2006: A Kuroshio Extension System model study: decadal chaotic self-sustained oscillations, J. Phys. Oceanogr., 36, 1605-1625.

——, 2008: On the crucial role of basin geometry in double-gyre models of the Kuroshio Extension. J. Phys. Oceanogr., 38, 1327–1333.

——, Dijkstra A.H., Riccio A., 2009: A nonlinear theory of the Kuroshio Extension bimodality, J. Phys. Oceanogr., 39, 2212-2229.

——, 2010: Coherence resonance in a double-gyre model of the Kuroshio Extension. J. Phys. Oceanogr., 40, 238–248, doi:10.1175/2009JPO4229.1.

——, 2011: Low-frequency variability, coherence resonance and phase selection in a low-order model of the wind-driven ocean circulation. J. Phys. Oceanogr., 41, 1585–1604, doi:10.1175/ JPO-D-10-05018.1.

——, 2012: Stochastic tipping points in climate dynamics. Phys. Rev., 85E, 027101, doi:10.1103/PhysRevE.85.027101.

——, 2014a: Kuroshio Extension Bimodality and the North Pacific Oscillation: A Case of Intrinsic Variability Paced by External Forcing. J. Climate, 27, 448–454.

——, 2014b: Ensemble Simulations and Pullback Attractors of a Periodically Forced Double-Gyre System, J. Phys. Oceanogr., 44, 3245–3254, 2014.

——, 2015: A Comparative Analysis of Kuroshio Extension Indices from a Modeling Perspective. J. Climate, 28, 5873-5881.

Pikovsky, A. S., and J. Kurths, 1997: Coherence resonance in noise-driven excitable systems. Phys. Rev. Lett., 78, 775– 778.

Qiu, B., 1995: Variability and energetics of the Kuroshio Extension and its recirculation gyre from the first two-year TOPEX data. J. Phys. Oceanogr., 25, 1827–1842.

——, 2000: Interannual variability of the Kuroshio Extension system and its impact on the wintertime SST field. J. Phys. Oceanogr., 30, 1486–1502.

——, and W. Miao, 2000: Kuroshio path variations south of Japan: Bimodality as a self-sustained internal oscillation. J. Phys. Oceanogr., 30, 2124–2137.

——, 2002: The Kuroshio Extension system: Its large-scale variability and role in the midlatitude ocean–atmosphere interaction. J. Oceanogr., 58, 57–75.

——, 2003: Kuroshio Extension variability and forcing of the Pacific decadal oscillations: Responses and potential feedback. J. Phys. Oceanogr., 33, 2465–2482.

——, Chen, S., 2005: Variability of the Kuroshio Extension jet, recirculation gyre and mesoscale eddies on decadal timescales. Journal of Physical Oceanography 35, 2090–2103.

——, and S. Chen, 2010: Eddy-mean flow interaction in the decadally-modulating Kuroshio Extension system. Deep-Sea Res. II, 57, 1097–1110, doi:10.1016/j.dsr2.2008.11.036.

Rayner, N. A., Parker, D. E.,Horton, E. B., Folland, C. K.,Alexander, L. V.,Rowell, D. P., Kent, E. C. and Kaplan, A., 2003: Global analyses of sea surface temperature, sea ice and night marine air temperature since the late nineteenth century. J. Geophys. Res.,108,4407

Rayner, N. A., Kennedy, J. J., Smith, R. O., and Titchner, H. A., 2016: The Met Office Hadley Centre Sea Ice and Sea Surface Temperature data set, version 2, part 3: the combined analysis, in preparation.

Roberts, M. J., Clayton, A., Demory, M.-E., Donners, J., Vidale, P. L., Shaffrey, L., Stevens, D. P., Stevens, I., Wood, R. A., and Slingo, J., 2009: Impact of Resolution on the Tropical Pacific Circulation in a Matrix of Coupled Models, J. Climate, 22, 2541-2556.

Sakamoto, T. T., Komuro, Y., Nishimura, T., Ishi, M., Tatebe, H., Shiogama, H., Hasegawa, A., Toyoda, T., Mori, M., Suzuki, T., Imada, Y., Nozawa, T., Takata, K., Mochizuki, T., Ogochi, K., Emori, S., Hasumi, H., and Kimoto, M., 2012: MIROC4h – A New High-Resolution Atmosphere-Ocean Coupled General Circulation Model, J. Meteorol. Soc. Jpn., 90, 325–359, doi:10.2151/jmsj.2012-301.

Sarkar, N. & Chaudhuri, B. B., 1994: An efficient differential box-counting approach to compute fractal dimension of image. IEEE Trans. Syst. Man. Cybern. 24, 115–120.

Sasaki Y.N., Schneider N., 2011: Decadal Shifts of the Kuroshio Extension Jet: Application of Thin-Jet Theory, J. Phys. Oceanogr., 41, 979-993.

Schubert, S. & Lucarini, V., 2016: Dynamical analysis of blocking events: spatial and temporal fluctuations of covariant lyapunov vectors. Q. J. R. Meteorol. Soc. 142, 2143–2158.

Schneider, N., A. J. Miller, and D. W. Pierce, 2002: Anatomy of North Pacific decadal variability. J. Climate, 15, 586–605.

——, and B. Cornuelle, 2005: The forcing of the Pacific decadal oscillation. J. Climate, 18, 4355–4373.

Schmeits, M. J., and H. A. Dijkstra, 2001: Bimodal behavior of the Kuroshio and the Gulf Stream. J. Phys. Oceanogr., 31, 3435–3456, https://doi.org/10.1175/1520-0485(2001)031,3435: BBOTKA.2.0.CO;2.

Sérazin, G., Penduff, T., Grégorio, S., Barnier, B., Molines, J. M., and Terray, L., 2015: Intrinsic variability of sea-level from global 1/12◦ ocean simulations: spatio-temporal scales, J. Climate, 28, 4279– 4292.

——, A. Jaymond, S. Leroux, T. Penduff, L. Bessieres, W. Llovel, B. Barnier, J.-M. Molines, and L. Terray, 2017: A global probabilistic study 1042 of the ocean heat content low-frequency variability: Atmospheric forcing 1043 versus oceanic chaos, Geophys. Res. Lett., 44, 55805589.

——, T. Penduff, B. Barnier, J.M. Molines, L. Terray, and B. Arbic, 2018: Inverse cascades of kinetic energy as a source of low-frequency 1046 intrinsic

variability: a global OGCM study. J. Phys. Oceanogr., 48, 1047 13851408, https://doi.org/10.1175/JPO-D-17-0136.1

Small, R. J., Bacmeister, J., Bailey, D. A., Baker, A., Bishop, S., Bryan, F. O., Caron, J., Dennis, J., Gent, P. R., Hsu, H.-M., Jochum, M., Lawrence, D. M., Munoz Acevedo, E., diNezio, P., Scheitlin, T., Tomas, R., Tribbia, J., Tseng, Y., and Vertenstein, M., 2014: A new synoptic-scale resolving global climate simulation using the Community Earth System Model, J. Adv. Model. Earth Syst., 6, 1065–1094, doi:10.1002/2014MS000363.

Taguchi, B., Xie, S., Mitsudera, H., & Kubokawa, A., 2005: Response of the Kuroshio Extension to Rossby Waves Associated with the 1970s Climate Regime Shift in a High-Resolution Ocean Model. Journal of Climate, 18(15), 2979-2995. Retrieved from http://www.jstor.org/stable/26253630

——, S.-P. Xie, N. Schneider, M. Nonaka, H. Sasaki, and Y. Sasai, 2007: Decadal variability of the Kuroshio Extension: Observations and an eddy-resolving model hindcast. J. Climate, 20, 2357–2377.

Tsujino, H., N. Usui, and H. Nakano, 2006: Dynamics of Kuroshio path variations in a high-resolution general circulation model. J. Geophys. Res., 111, C11001, https://doi.org/10.1029/2005JC003118.

——, S. Nishikawa, K. Sakamoto, N. Usui, H. Nakano, and G. Yamanaka, 2013: Effects of large-scale wind on the Kuroshio path south of Japan in a 60-year historical OGCM simulation. Climate Dyn., 41, 2287–2318, https://doi.org/ 10.1007/s00382-012-1641-4.

Vallis, G. K., 2006: Atmospheric and Oceanic Fluid Dynamics. Cambridge University Press, 745 pp.

Vannière, B., Demory, ME., Vidale, P.L. et al. Clim Dyn, 2019: Multi-model evaluation of the sensitivity of the global energy budget and hydrological cycle to resolution. 52, 6817. https://doi.org/10.1007/s00382-018-4547-y

Wang, Y., Yang, X. & Hu, 2016: Position variability of the Kuroshio Extension sea surface temperature front, J. Acta Oceanol. Sin, 35, 30. https://doi.org/10.1007/s13131-016-0909-7

Wei, Y., Yang, X. & Hu, J. Acta Oceanol. Sin., 2016: Position variability of the Kuroshio Extension sea surface temperature front. 35: 30. https://doi.org/10.1007/s13131-016-0909-7

——, Zhang, RH. & Wang, H. J Oceanogr, 2017: Mesoscale wind stress–SST coupling in the Kuroshio extension and its effect on the ocean. 785. https://doi.org/10.1007/s10872-017-0432-2; 73.

Huang, B., V.F. Banzon, E. Freeman, J. Lawrimore, W. Liu, T.C. Peterson, T.M. Smith, P.W. Thorne, S.D. Woodruff, and H.-M. Zhang, 2014: Extended Reconstructed Sea Surface Temperature version 4 (ERSST.v4): Part I. Upgrades and intercomparisons. Journal of Climate, 28, 911–930, doi:10.1175/JCLI-D-14-00006.1.

Wu, R. and Kirtman, B. P., 2007: Regimes of seasonal air-sea interaction and implications for performance of forced simulations, Clim. Dynam, 29, 393–410, doi:10.1007/s00382-007-0246-9.

Wyrtki, K., L. Magaard, and J. Hagar, 1976: Eddy energy in the oceans. J. Geophys. Res., 81, 2641–2646.

Yang, Y., and X. S. Liang, 2016: The instabilities and multiscale energetics underlying the mean–interannual–eddy interactions in the Kuroshio Extension region. J. Phys. Oceanogr., 46, 1477– 1494, https://doi.org/10.1175/JPO-D-15-0226.1.

——, and ——, 2019: The intrinsic nonlinear multiscale interactions among the mean flow, low frequency variability and mesoscale eddies in the Kuroshio region. Sci. China Earth Sci., 62, 595–608, https://doi.org/10.1007/s11430-018-9289-4.

——, ——, B. Qiu, and S. Chen, 2017: On the decadal variability of the eddy kinetic energy in the Kuroshio Extension. J. Phys. Ocean- ogr., 47, 1169–1187, https://doi.org/10.1175/JPO-D-16-0201.1.

Yasuda, I., J.-H. Yoon, and N. Suginohara, 1985: Dynamics of the Kuroshio large meander. J. Oceanogr. Soc. Japan, 41, 259–273, https://doi.org/10.1007/BF02109275.

Yoon, J.-H., and I. Yasuda, 1987: Dynamics of the Kuroshio large meander: Two-layer model. J. Phys. Oceanogr., 17, 66–81, https://doi.org/10.1175/1520-0485(1987)017,0066: DOTKLM.2.0.CO;2.

Yu, L., X. Jin, and R. A. Weller, 2008: Multidecadal global flux datasets from the Objectively Analyzed Air–Sea Fluxes (OAFlux) Project: Latent and sensible heat fluxes, ocean evaporation, and related surface meteorological variables. Woods Hole Oceanographic Institution, OAFlux Project Tech. Rep. OA-2008-01, 64 pp. [Available online at http://oaflux.whoi.edu/.]

Zhang J. & Luo D.H., 2017: Impact of Kuroshio Extension dipole mode variability on the North Pacific storm track, Atmospheric and Oceanic Science Letters, 10:5, 389-396, DOI: 10.1080/16742834.2017.1351864.

Student: Giusy Fedele **matricola: 956305**

PhD in: Science and Management of Climate Change

Cicle: 32

Abstract

The Kuroshio Extension (KE) is the inertial meandering jet formed by the convergence of the Kuroshio and Oyashio currents in the Northern Pacific.

It is widely mentioned in the literature that the KE variability is bimodal on interannual to decadal time scales. The nature of this low frequency variability (LFV) is still under debate; some authors suggest that internal oceanic mechanisms play a fundamental role in the phenomenon but there is also evidence from the observations that the KE LFV is connected with changes in broader patterns of variability such as the Pacific Decadal Oscillation (PDO).

In this thesis we first inspect the interplay between the ocean and the atmosphere in the KE, taking advantage of a large ensemble of global hindcasts and finally, we examine the role of the atmosphere in the KE's total variability in the context of a fully coupled system.

We show in agreement with previous studies that the KE LFV is an intrinsic oceanic mechanism paced by atmospheric forcings and that changes in the horizontal resolution of the atmospheric model have not a relevant impact on the KE's degree of realism. In this context, we highlight that the PDO acts as a pacemaker of the KE LFV, suggesting this pattern as a predictor.

With this study we have made some progress in the state-of-the-art and the current scientific knowledge, understanding both the nature of the KE LFV and the impacts of the atmospheric horizontal resolution on the KE system, which is important to identify the needs of the next generation models to capture and predict the KE LFV.

Studente: Giusy Fedele **matricola: 956305**

Dottorato in: Scienze e gestione dei cambiamenti climatici

Ciclo: 32

Estratto

L'Estensione del Kuroshio (KE) è il getto inerziale formato dalla convergenza delle correnti Kuroshio e Oyashio nel Pacifico settentrionale.

È ampiamente menzionato in letteratura che la variabilità del KE è bimodale su scale temporali interannuali-decadali. La natura di questa variabilità a bassa frequenza (LFV) è ancora in discussione; alcuni autori suggeriscono che meccanismi oceanici interni svolgono un ruolo fondamentale nel fenomeno, ma allo stesso tempo le osservazioni mostrano che il KE LFV è connesso a pattern di variabilità su ampia scala come l'Oscillazione del Pacifico Decadale (PDO).

In questa tesi inizialmente esaminiamo l'interazione tra oceano e atmosfera nel KE, sfruttando un ensemble di hindcasts globali, dopodiché investighiamo il ruolo dell'atmosfera nella variabilità totale del KE nel contesto di un sistema completamente accoppiato.

Mostriamo in accordo con studi precedenti che il KF LFV è un meccanismo oceanico intrinseco eccitato da forzanti atmosferici e che cambiamenti nella risoluzione orizzontale del modello atmosferico non hanno un impatto rilevante sul grado di realismo del KE. In questo contesto, evidenziamo che il PDO agisce come pacemaker del KE LFV, suggerendo questo pattern come predittore.

Con questo studio abbiamo compiuto alcuni progressi nello stato dell'arte e nelle attuali conoscenze scientifiche, comprendendo sia la natura del KE LFV, sia gli impatti della risoluzione orizzontale atmosferica sul jet, al fine di individuare le esigenze dei modelli di prossima generazione nella simulazione e previsione di questo sistema dinamico.